

1 *Response to the reviewer*

2

3 *I appreciate the comments of the reviewer and explaining the ideas underlying the study of Kollet*  
4 *and Maxwell (2006). Below I have copied all the comments and have inserted my replies in italics.*

5

6 I think that the manuscript underwent improvements and got more focused, which is good. There  
7 are some structural problems (results, discussion, conclusions are in the introduction, see specific  
8 comments below) and language problems. In addition some additional clarification would help the  
9 reader.

10 Going back to original publication by Kollet and Maxwell (2006), I feel the paper's important point  
11 and novelty was not on a numerical approach (common or dual node or something else). The  
12 important point was the realization that the kinematic wave equation can be merged into the top  
13 flux boundary condition resulting in a free surface boundary condition at the land surface, very  
14 similar to the one used to obtain analytical solutions for a pumping test in unconfined aquifers. I  
15 feel this was really the message and as such it can be implemented in a model (numerical, perhaps  
16 even semi-analytical and analytical) in a consistent fashion to mathematically close the problem  
17 of subsurface flow as the authors wrote. Unfortunately, the numerical implementation is not very  
18 clear from the paper, but the sensitivity to the vertical discretization, which clearly is a  
19 disadvantage in case of excess infiltration, was transparently reported in the numerical test cases.  
20 Yet, this does not detract from the theoretical and practical appeal of the free surface overland flow  
21 boundary condition proposed in this paper. I feel that is something that should be pointed out in  
22 the ensuing revision of this manuscript. Note also the term “common node” approach was not  
23 introduced by Kollet and Maxwell.

24 *As said, I appreciate this detailed explanation about the ideas underlying the paper of Kollet and*  
25 *Maxwell (2006). Let me start with the terms dual and common nodes. It is true that these terms do*  
26 *not appear in the paper. However, they have been used to distinguish between the two coupling*  
27 *approaches, most notably by the people who developed the code HydroGeoSphere. In my opinion*  
28 *the terms are very appropriate as they are short and self-explanatory. It is true, that originally*  
29 *these terms apply to vertex-centered schemes. But once the cell center in a cell-centered scheme*  
30 *is defined as a ‘node’, then the terms can also be applied to cell-centered schemes.*

31 *In my opinion, I clearly mentioned that the key advantages (theoretical and practical) of the idea*  
32 *of Kollet and Maxwell (2006). Namely in the introduction, I mention that the idea avoids the*  
33 *introduction of a coupling length / exchange parameter. Avoiding this model parameter is an*  
34 *advantage as it is often believed to be a non-physical parameter. A key point of my study is,*  
35 *however, is that this model parameter should be a function of the vertical discretization. Moreover,*  
36 *as I discussed, the way of enforcing head continuity at the surface in the common node approach*  
37 *is somewhat problematic.*

38

39

40 I am surprised by the (sometimes) large difference in non-linear iterations, because in principle the  
41 common node and dual nodes approach are very similar (which is also the reason why they can be  
42 easily switched in the code as described in the manuscript). Which additional nonlinearity is  
43 introduced in case of the common node approach? A more satisfactory attempt of explaining this  
44 phenomenon would be needed in my opinion.

45 *In my opinion this is actually well explained in the manuscript (section 6). But I agree, that if one*  
46 *is focusses on the similarities between the coupling approaches, the differences are somewhat*  
47 *surprising. In fact it is not related to differences in non-linearities, but to rates at which the flow*  
48 *variables are changing around the moment that ponding is initiated. At this time the system*  
49 *displays a discontinuity in flow behavior as surface flow terms are about to be activated*  
50 *(regardless of the coupling approach). The higher the rate at which the flow variables are*  
51 *changing, the more difficult the solution will be. As discussed in section 6 and illustrated by*  
52 *figures, the common node approach is characterized by higher rates and is thus more difficult to*  
53 *solve. These differences in the rate only occur during a short moment but exactly at the moment*  
54 *that the system is difficult to solve. Going a bit further, the differences in the rate of change are*  
55 *related to the condition for ponding to start. The crux here is that the common node approach*  
56 *requires fully saturated conditions for ponding to occur. That means that just before ponding the*  
57 *rate of change in the pressure head is quite high.*

58 Provided the general comments above and more specific comments below, I am recommending  
59 minor revisions.

60 68: Is Kollet and Maxwell (2006) and appropriate reference for MODHMS?

61 *Corrected*

62 100 - 127: These are results and discussion/summary/conclusions and do not belong in the  
63 introduction section.

64 *In my opinion this is not the case. Namely, an important part of my study focusses on how the dual*  
65 *node approach should be implemented and this should be clear from the introduction.*  
66 *Furthermore that part of the work builds on the work of others (An and Yu, Panday and Huyakorn).*  
67 *Those previous studies should thus be referenced in the introduction.*

68 137: ...the mesh...

69 *Corrected*

70 220: What is fp in the equation?

71 Line 187: the fraction of the interface that is ponded. But I noticed that the p index was in italics.  
72 That was incorrect.

73 232: ...dua nodes. The infiltration...

74 *Rephrased*

75

76 292: I am confused and not sure what the authors wants get at. When  $q_r = I$  then  $q_r = Kz$ , thus  $p_{ss} = 0$ , because there is a unit gradient at the right at the land surface. If  $p_{ss} < 0$  then  $q_r < I$ , contrary to equation 8 because  $p_s$  is not zero. In case of  $q_r > I$ , again  $q_s$  is not equal zero and  $p_{ss} < 0$  is wrong in this case. The physics and transient pressure behavior near the surface right at the onset of ponding is more complicated and has been discussed extensively in the literature (Kutilek and Nielsen). Storativity concepts need to be introduced if I remember correctly. If the author wants to look at these processes in the some limit, then this should be done in a mathematically rigorous fashion in my opinion.

84 *I have changed this paragraph. I think it is now more clear what I want to get at. In particular, I*  
85 *make it more clear where the  $p_s = 0$  is coming from.*

86 376:

87 380: necessarily

88 *Corrected*

89 441: Kollet and Maxwell also showed that in their original publication, no?

90 *Corrected*

91 In figure 4 and 5, it is very difficult to distinguish between the  $d_n$  and  $c_n$  results.

92 *Corrected (using dashed lines for common node plots)*

93 Make sure to carefully check language and grammar, especially for typos.

94

95

96

97

98

99

100

101

102

103

104

105 **New insights into the differences between the dual node approach**  
106 **and the common node approach for coupling surface-subsurface**  
107 **flow**

108

109 Rob de Rooij

110 Water Institute, University of Florida, 570 Weil Hall, PO Box 116601, Gainesville, FL-32611-

111 6601, USA

112 r.derooij@ufl.edu

113

114 Corresponding author:

115 Rob de Rooij

116 Water Institute

117 University of Florida

118 570 Weil Hall

119 PO Box 116601

120 Gainesville

121 FL-32611-6601

122 USA

123 Telephone: 1-352-392-5893

124 Fax: 1-352-392-6855

125 **Key points**

126 Surface-subsurface flow coupling

127

128

129

130

131

132

133

134

135

136

137

138

139

140

141

142

143

144

145

146 **Abstract**

147 The common node approach and the dual node approach are two widely applied approaches to  
148 couple surface-subsurface flow. In this study both approaches are analyzed for cell-centered as  
149 well as vertex-centered finite difference schemes. It is shown that the dual node approach should  
150 be conceptualized and implemented as a one-sided first-order finite-difference to approximate the  
151 vertical subsurface hydraulic gradient at the land surface. This results in a consistent dual node  
152 approach in which the coupling length is related to grid topology. In this coupling approach the  
153 coupling length is not to be interpreted as a non-physical model parameter. Although, this  
154 particular coupling approach is technically not new, the differences between this consistent dual  
155 node approach and the common node approach have not been studied in detail. In fact, this  
156 coupling scheme is often believed to be similar to the common node approach. In this study it is  
157 illustrated that in comparison to the common node approach, the head continuity at the surface-  
158 subsurface interface is formulated more correctly in the consistent dual node approach. Numerical  
159 experiments indicate that the consistent dual node approach is less sensitive to the vertical  
160 discretization when simulating excess infiltration. It is also found that the consistent dual node  
161 approach can be advantageous in terms of numerical efficiency.

162

163

164

165

166

167 **1 Introduction**

168 There exists a variety of hydrogeological problems, such as the hydrologic response of hillslopes  
169 and river catchments, which requires an integrated analysis of surface and subsurface flows. This  
170 has led to the development of physically-based, distributed parameter models for simulating  
171 coupled surface-subsurface flows. Well-known examples of such models include MODHMS  
172 [~~Kollet and Maxwell, 2006~~; Panday and Huyakorn, 2004] , InHM [Ebel et al., 2009],  
173 HydroGeoSphere [Therrien et al., 2010], CATHY [Camporese et al., 2010], WASH123D [Yeh et  
174 al., 2011], ParFlow [Kollet and Maxwell, 2006] and OpenGeoSys [Kolditz and Shao, 2010].  
175 Typically, subsurface flow is governed by the Richards' equation whereas surface flow is either  
176 governed by the kinematic wave or the diffusive wave equation.

177         The coupling between subsurface and surface flow may be either based on the common  
178 node approach [Kollet and Maxwell, 2006] or on the dual node approach [Ebel et al., 2009; Panday  
179 and Huyakorn, 2004; VanderKwaak, 1999]. In the common node approach coupling is formulated  
180 by a continuity in head between surface and subsurface nodes. The dual node approach is based  
181 on formulating an exchange flux between the surface and subsurface nodes. Typically, the dual  
182 node approach is conceptualized as a hydraulic separation of the surface and the subsurface by an  
183 interface with a given thickness [Liggett et al., 2012]. The thickness of this interface defines a  
184 coupling length between the dual nodes to formulate the discrete exchange flux between the dual  
185 nodes.

186         It has been argued that the coupling length represents a non-physical model parameter,  
187 because there is often no evidence to support the existence of a distinct interface between the two  
188 flow domains [Kollet and Maxwell, 2006]. As such it appears that the common node approach is  
189 a more physically based coupling approach [Kollet and Maxwell, 2006; Liggett et al., 2012]. It has

190 also been found that accurate simulations based on the dual node approach typically require a very  
191 small coupling length [Ebel *et al.*, 2009; Liggett *et al.*, 2012; Liggett *et al.*, 2013]. Since it is known  
192 that the dual node approach mimics the common node in the limit as the coupling length goes to  
193 zero [Ebel *et al.*, 2009], it thus seems that the dual node approach is most accurate if it mimics the  
194 common node approach. Nonetheless, it has been argued that the dual node approach remains an  
195 attractive alternative coupling approach since it offers more flexibility than the common node  
196 approach. Namely, while it can mimic the common node approach, the dual node approach offers  
197 the possibility to simulate a less tight coupling of surface-subsurface flow which results in  
198 increased computational efficiency [Ebel *et al.*, 2009].

199 In this study a detailed analysis of both coupling approaches is provided for cell-centered  
200 as well as vertex-centered finite difference schemes. This analysis starts with the crucial  
201 observation that that the topmost subsurface nodal values as computed by the finite difference  
202 schemes represent the mean values within the topmost discrete control volumes. Numerical  
203 experiments to compare the coupling approaches are carried out with the model code DisCo [de  
204 Rooij *et al.*, 2013]. It is shown that the dual node approach should be interpreted and implemented  
205 as a one-sided finite difference approximation of the vertical hydraulic gradient at the land surface.  
206 This yields a consistent dual node scheme in which the coupling length is defined by the half the  
207 thickness of the topmost subsurface cells. The scheme of An and Yu [An and Yu, 2014] as well as  
208 the scheme of Kumar *et al.* [Kumar *et al.*, 2009] are essentially very similar to this consistent dual  
209 node scheme. In the work of Panday and Huyakorn [Panday and Huyakorn, 2004], one of the  
210 suggestions to define the coupling length is to use half the thickness of the topmost subsurface  
211 cells, which yields a consistent dual node scheme. While the idea that the coupling length can be  
212 based on the grid topology is not new [Panday and Huyakorn, 2004], the idea that it must be



213 related to grid topology to obtain a consistent approach is a significant new insight. Namely, since  
214 the coupling length in the consistent dual node approach is not to be interpreted as the thickness  
215 of a layer that separates the subsurface from the surface, the consistent dual node approach is not  
216 automatically less physically based than the common node. In fact, as explained in this study in  
217 comparison to the common node approach the implementation of a head continuity at the surface-  
218 subsurface interface is formulated more correctly in the consistent dual node approach.

219         The current consensus about how the dual node approach compares to the common node  
220 approach is based on alternative dual node approaches which as explained in this study are  
221 different from the consistent dual node approach. In this study the consistent dual node approach  
222 is compared in detail with the common node approach. It is shown that if the vertical discretization  
223 is sufficiently fine, then the common node approach and the consistent dual node approach are  
224 equally accurate. However, when simulating excess infiltration the consistent dual node approach  
225 is found to be less sensitive to the vertical discretization in comparison to the common node  
226 approach. This advantage in accuracy is related to the fact that head continuity is more correctly  
227 formulated in the consistent dual node approach. Moreover, it is also shown that the consistent  
228 dual node approach can be advantages in terms of numerical efficiency when simulating runoff  
229 due to both excess saturation as well as excess infiltration. The finding of this study show that the  
230 consistent dual node approach compares more positively with respect to the common node  
231 approach than other dual node approaches.

## 232 **2 Interpretation of nodal values**

233 As explained later on, a correct interpretation of nodal values is crucial for understanding the dual  
234 and common node approach for coupling surface-subsurface flow. Moreover, both coupling

235 approaches depend on the configuration of surface and topmost subsurface nodes near the land  
236 surface. This configuration depends on whether cell-centered or vertex-centered schemes are used.  
237 In this study both type of schemes will be covered, but for simplicity only finite difference schemes  
238 are considered.

239 In both cell-centered as vertex-centered schemes the flow variables such as the heads and  
240 the saturation are computed on nodes. In vertex-centered schemes these nodes coincide with the  
241 vertices of the mesh, whereas in cell-centered schemes the nodes coincide with the cell centers.  
242 When employing a finite difference scheme, nodal values correspond to the mean value within  
243 surrounding discrete control volumes. In cell-centered finite difference schemes these discrete  
244 volumes are defined by the primary grid cells. In vertex-centered finite difference schemes these  
245 discrete volumes are defined by the dual grid cells. Ideally, the mean values in the discrete control  
246 volumes are derived by applying the midpoint rule for numerical integration such that their  
247 approximation is second-order accurate. Therefore, the nodal values should ideally represent  
248 values at the centroid of the surrounding discrete control volume [Blazek, 2005; Moukalled *et al.*,  
249 2016]. In that regard, a cell-centered finite difference scheme is thus more accurate than a vertex-  
250 centered finite difference scheme. Namely, in cell-centered finite difference schemes the nodal  
251 values always correspond to the centroids of the cell whereas in vertex-centered finite difference  
252 schemes nodes and centroids (of the dual cells) do not coincide at model boundaries and in model  
253 regions where the primary grid is not uniform. It is well-known that this mismatch between nodes  
254 and centroids can lead to inaccuracies since the mean values within affected discrete volumes are  
255 not computed by a midpoint rule [Blazek, 2005; Moukalled *et al.*, 2016].

256 Typically, vertex-centered schemes for simulating coupled surface-subsurface flow are  
257 based on mass-lumped finite element schemes [Liggett *et al.*, 2012] and not on finite difference

258 schemes. However, with respect to coupling surface-subsurface flow there is actually no difference  
259 between a mass-lumped finite element scheme and a vertex-centered finite difference scheme.  
260 Similar as in vertex-centered finite difference schemes, the nodal values in mass-lumped finite  
261 element schemes define the mean values inside dual grid cells [Zienkiewicz *et al.*, 2005].  
262 Moreover, the coupling approaches establish one-to-one relations between surface and topmost  
263 subsurface nodes which do not depend on whether a finite difference or a finite element approach  
264 is being used.

### 265 **3 Common node approach**

266 The common node approach defines a head continuity between the topmost subsurface nodes and  
267 the surface nodes. This continuity requires that the topmost subsurface nodes and the surface nodes  
268 are co-located at the land surface such that there exists a continuity in the elevation head. This  
269 requirement is automatically full-filled in vertex-centered schemes. Figure 1a illustrates the  
270 configuration of common nodes in ParFlow, a cell-centered scheme [personal communication  
271 Maxwell, R. in relation to previous work of the author [De Rooij *et al.*, 2012]]. Figure 1c illustrates  
272 the configuration of common nodes for vertex-centered schemes. This configuration is similar to  
273 the configuration as used in HydroGeoSphere [Therrien *et al.*, 2010].

274         Considering that nodal values represent ideally the mean values within discrete control  
275 volumes as described in Section 2, it can be argued that the head continuity as implemented in the  
276 common node approach is not in agreement with the physical principle of head continuity at the  
277 land surface. Namely, the common node approach enforces a continuity between surface heads at  
278 the land surface and the mean subsurface heads within the topmost subsurface discrete control  
279 volumes which have a finite thickness. This is different from enforcing a continuity between

280 surface heads and subsurface heads within an infinitesimal thin subsurface layer directly below the  
281 land surface. As such the common node approach is only numerically correct if the topmost  
282 subsurface cells are very thin.

## 283 **4 Dual node approach**

### 284 **4.1 Basics**

285 Figure 1b and 1c illustrate the classical arrangement of surface and subsurface nodes in cell-  
286 centered and vertex-centered finite difference schemes, respectively. Commonly, the dual node  
287 approach is expressed in terms of an exchange flux  $q_e$  [ $\text{LT}^{-1}$ ] computed as [*Liggett et al.*, 2012;  
288 *Panday and Huyakorn*, 2004]:

$$289 \quad q_e = f_p \frac{K_z}{l} (h_s - h_{ss}) \quad (1)$$

290 where  $h_s$  and  $h_{ss}$  are the hydraulic heads [L] associated with the surface node and the topmost  
291 subsurface node, respectively,  $f_p$  [-] the fraction of the interface that is ponded and  $l$  the coupling  
292 length [L]. The ponded fraction of the interface is typically defined by a function that varies  
293 smoothly between zero at the land surface elevation and unity at the rill storage height which  
294 defines the minimum water depth for initiating lateral overland flow [*Panday and Huyakorn*,  
295 2004]. In equation (1) the term  $f_p K_z / l$  is commonly referred to as the first-order exchange  
296 parameter, where first-order means that the exchange flux depends linearly of the hydraulic head  
297 difference.

298 Typically, equation (1) is not derived as a numerical approximation of basic flow equations  
299 that govern the exchange flux, but is merely presented a numerical technique to couple two  
300 different flow domains [*Ebel et al.*, 2009; *Liggett et al.*, 2012]. Subsequently, the dual node

301 approach is conceptualized by interpreting equation (1) as an expression that describes  
 302 groundwater flow across a distinct interface separating the two flow domains [Ebel *et al.*, 2009;  
 303 Liggett *et al.*, 2012; Liggett *et al.*, 2013].

#### 304 4.2 Consistent dual node approach

305 In the following, it is illustrated that the dual node approach can and should be derived from basic  
 306 equations that describe infiltration into a porous medium. Using Darcy's Law, the infiltration rate  
 307 at the ponded land surface  $q_{s \rightarrow ss}$  [ $LT^{-1}$ ] can be written as a function of the vertical subsurface  
 308 hydraulic gradient at the land surface:

$$309 \quad q_{s \rightarrow ss} = \left( k_r K_z \frac{\partial h}{\partial z} \right) \Big|_{z=z_s} = K_z \frac{\partial h}{\partial z} \Big|_{z=z_s} \quad (2)$$

310 where  $h$  the hydraulic head [L],  $z$  the elevation head [L],  $k_r$  the relative hydraulic conductivity [-]  
 311  $K_z$  the saturated vertical hydraulic conductivity [ $LT^{-1}$ ] and  $z_s$  the elevation head at the land surface.  
 312 The relative hydraulic conductivity is unity because equation (2) applies to the ponded land surface  
 313 which implies fully saturated conditions at the land surface (i.e. ponding means  $p_s > 0$ , where  $p_s$  is  
 314 the pressure head at the surface). Similarly, the infiltrability [ $LT^{-1}$ ], defined as the infiltration rate  
 315 under the condition of atmospheric pressure [Hillel, 1982], can be written as:

$$316 \quad I = \left( k_r K_z \frac{\partial h}{\partial z} \right) \Big|_{z=z_s, p_s=0} = K_z \frac{\partial h}{\partial z} \Big|_{z=z_s} \quad (3)$$

317 The relative hydraulic conductivity is again unity because the saturation equals unity under  
 318 atmospheric conditions ( $p_s = 0$ ). The infiltration rate at non-ponded land surface  $\underline{q_{atm \rightarrow ss}}$  [ $LT^{-1}$ ] can  
 319 be expressed as:

$$320 \quad q_{atm \rightarrow ss} = \min(\max(I, 0), q_R) \quad (4)$$

321 where  $q_R$  is the effective rainfall rate (i.e. the infiltration rate is limited by either the infiltrability  
 322 or the available effective rainfall rate). The total exchange flux across the surface-subsurface  
 323 interface can now be written as:

$$324 \quad \cancel{q_c} = \cancel{f_p} q_{s \rightarrow ss} + \cancel{(1 - f_p)} q_{atm \rightarrow ss} \quad \underline{q_c = f_p q_{s \rightarrow ss} + (1 - f_p) q_{atm \rightarrow ss}} \quad (5)$$

325 To approximate the vertical subsurface hydraulic gradient in equations (2) and (3) , it is  
 326 crucial to recognize that according to the principle of head continuity at the land surface, the  
 327 surface hydraulic head at a surface node must also represent the subsurface head at the land surface  
 328 at that location. Moreover, since the subsurface hydraulic heads at the topmost subsurface nodes  
 329 are ideally associated with the centroids of the topmost subsurface discrete control volumes, these  
 330 head values do not represent values at the land surface but at some depth below the land surface.  
 331 Because the subsurface hydraulic heads at the dual nodes can be and should be associated with a  
 332 different elevation, the vertical subsurface head gradient between the dual nodes can be  
 333 approximated by a standard finite difference approximation. If this approximation is being used to  
 334 approximate the gradient at the land surface in equations (2) and (3), then this approximation is by  
 335 definition a one-sided first-order finite difference. **By** defining the coupling length by  $l = \Delta z_{dn}$   
 336 where  $\Delta z_{dn}$  is the difference in the mean elevation head associated with the dual nodes, the  
 337 infiltration rate and infiltrability can thus be computed with the following one-sided finite  
 338 difference approximation:

$$339 \quad K_z \left. \frac{\partial h}{\partial z} \right|_{z=z_s} \approx \frac{K_z}{l} (h_s - h_{ss}) \quad (6)$$

340 The above definition of the coupling length  $l = \Delta z_{dn}$  ensures a proper approximation of the vertical  
 341 gradient in elevation head at the land surface:

342 
$$\left. \frac{\partial z}{\partial z} \right|_{z=z_s} = \frac{\Delta z_{\text{dn}}}{l} = 1 \quad (7)$$

343 The above derivation of the consistent dual node approach from basic flow equations has  
344 implications for how the dual node approach is conceptualized and how it should be implemented.  
345 The idea that the coupling length must be directly related to the spatial discretization is an  
346 important new insight. Namely, as the coupling length is related to grid topology, it does not  
347 represent a non-physical parameter associated with a distinct interface separating the two domains.  
348 It is also crucial to observe the difference between the consistent dual node approach and the  
349 common node approach regarding how the head continuity at the surface-subsurface interface is  
350 formulated. As explained in Section 2, the formulation in the common node approach is only  
351 correct if the topmost subsurface discrete volumes are very thin. In comparison, the formulation  
352 in the dual node approach is correct irrespective of the vertical discretization. Namely, irrespective  
353 of the vertical discretization the surface hydraulic heads equal the subsurface heads at the interface.

354 Since nodal values in cell-centered scheme are located at the centroids of the cells, the  
355 coupling length is simply given by  $l = z_s - z_{\text{ss}}$  where  $z_s$  and  $z_{\text{ss}}$  are the elevation heads [L] associated  
356 with the surface node and the topmost subsurface node, respectively. This value for the coupling  
357 length in cell-centered schemes has also been suggested by Panday and Huyakorn [*Panday and*  
358 *Huyakorn, 2004*]. However, in their work, the particular advantage of choosing this value (i.e.  
359 maintaining a unit gradient in elevation head) is not recognized. The coupling schemes as used by  
360 An and Yu [*An and Yu, 2014*] and Kumar et al. [*Kumar et al., 2009*] are also in essence consistent  
361 dual node schemes. However, these schemes are not recognized as a dual node scheme. Instead,  
362 An and Yu [*An and Yu, 2014*] argue that their scheme is similar to the common node approach of  
363 Kollet and Maxwell [*Kollet and Maxwell, 2006*]. Kumar et al. [*Kumar et al., 2009*] argue that their

364 scheme is similar to the dual node approach if the coupling length goes to zero which implies that  
365 their scheme would be similar to the common node approach. However, contrary to the common  
366 node approach the schemes of An and Yu [*An and Yu, 2014*] and Kumar et al. [*Kumar et al., 2009*]  
367 compute exchange fluxes between surface and topmost subsurface nodes and therefore these  
368 schemes are technically dual node schemes. As explained in this study, it is crucial to observe that  
369 the schemes of An and Yu [*An and Yu, 2014*] and Kumar et al. [*Kumar et al., 2009*] are actually  
370 quite different from the common node approach. As already mentioned, the consistent dual node  
371 scheme differs from the common node approach with respect to how the head continuity is  
372 formulated at the surface-subsurface interface. As discussed later on, this difference has crucial  
373 consequences in terms of accuracy as well as numerical efficiency.

374         In vertex-centered schemes the commonly used nodal configuration near the surface is such  
375 that  $z_s = z_{ss}$ . However, even though the topmost subsurface node is located at the land surface in a  
376 vertex-centered scheme, the elevation head at this node should ideally correspond to the mean  
377 elevation head within the topmost subsurface discrete volume. This suggests that the topmost  
378 subsurface node should be moved to the centroid of the topmost subsurface discrete volume.  
379 Although this is a possible solution, the drawback of this solution is that the subsurface model  
380 ceases to be a purely vertex-centered scheme. Moreover, such an operation cannot be performed  
381 in finite element schemes since the nodal positions define the geometry of the elements. Therefore,  
382 an alternative solution is proposed. Namely, in vertex-centered schemes the elevation of the  
383 surface nodes are changed according to  $z_s = z_{ss} + l$  where  $l$  is equals half the thickness of the  
384 topmost subsurface dual cell. The resulting nodal configuration is illustrated in Figure 1d. When  
385 applying this solution, all the topmost subsurface cells must have the same thickness, such that the  
386 topography is increased with the same value everywhere. In essence, the motivation behind this



387 solution is that a more accurate approximation the hydraulic gradient (i.e. enforcing a unit gradient  
 388 in elevation head) is more important than the actual elevation of the land surface. Similar to the  
 389 nodal configuration in ParFlow, the resulting nodal configuration may not seem ideal. Namely, the  
 390 surface elevation does not coincide with the top of the subsurface grid. Nonetheless, as illustrated  
 391 later on, simulation results obtained with the resulting scheme are reasonable.

392 To illustrate that the presented dual node approach exhibits consistent behaviour, the  
 393 necessary conditions for ponding due to excess infiltration and exfiltration are considered. In  
 394 general ponding starts when  $q_R > I$  [Hillel, 1982]. ~~Setting  $q_R = I$ ,  $p_s = 0$  and using  $h = p + z$ , it~~  
 395 ~~follows from~~ Observing that equation (6) and (7) that at the moment of ponding defines the  
 396 computed infiltrability when  $p_s = 0$  and that the gradient in elevation head between the dual nodes  
 397 is unity, the infiltrability can be expressed by  $I = K_z (1 - p_{ss}/l)$ . Therefore,  $q_R > I$  implies that:

$$398 \quad p_{ss} = l \left( 1 - \frac{q_R}{K_z} \right) \quad p_{ss} > l \left( 1 - \frac{q_R}{K_z} \right)$$

399 (8)

400 Ponding due to excess infiltration occurs if  $q_R/K_z > 1$  and implies that saturation in the subsurface  
 401 starts from the top down [Hillel, 1982]. Using  $q_R/K_z > 1$  it follows from equation (8) that  $p_{ss}$  is  
 402 still negative at the moment of ponding ~~due to excess infiltration occurs while  $p_{ss} < 0$ .~~ This is  
 403 reasonable ~~since this value represents, because~~ the pressure head value at the topmost subsurface  
 404 node represents a value at a certain depth below the land surface. ~~Namely, if~~ Top-down saturation  
 405 ~~occurs from the top down then the saturation at a certain depth occurs later than~~ implies that  
 406 saturation at the ~~land surface~~ topmost subsurface node occurs after ponding and thus a negative  
 407 pressure head value at this node at the moment that ponding starts. It is noted that if the ratio  $q_R/K_z$

408 is greater than but close to unity or if the coupling length is very small, then this condition becomes  
 409  $p_{ss} \approx 0$ . Once ponding starts the total flux rate between the dual nodes equals  $K_z ((p_s - p_{ss})/l + 1)$   
 410 . Top-down saturation requires that this flux exceeds the vertical hydraulic conductivity. Reaching  
 411 saturation at the topmost node ( $p_{ss} = 0$ ) therefore requires  $p_s \geq 0$ . Thus, ~~top-down~~ while  $p_{ss}$  is still  
 412 negative at the moment that ponding starts, saturation at the topmost subsurface node will occur  
 413 some time after ponding ~~is initiated~~ started. Ponding due to excess saturation occurs if  $q_R/K_z < 1$   
 414 and implies that saturation in the subsurface starts from the bottom up [Hillel, 1982]. It follows  
 415 from equation (8) that ponding due to excess saturation occurs while  ~~$0 < p_{ss} < l$~~   $p_{ss} > 0$ . Thus  
 416 ponding starts after reaching fully saturated conditions at the topmost subsurface node, which is  
 417 again reasonable. It is noted that if the ratio  $q_R/K_z$  is smaller than but close to unity or if the  
 418 coupling length is very small, then ponding occurs when  $p_{ss} \approx 0$ .

### 419 4.3 Comparison to alternative coupling approaches

420 To illustrate that it is crucial to account for the meaning of the values at the topmost subsurface  
 421 nodes, it is instructive to consider what happens if these values are not taken as the mean values  
 422 within discrete control volumes. As a first example, consider vertex-centered schemes where the  
 423 dual nodes are defined such that  $z_{ss} = z_s$  as illustrated in Figure 1c. This is inconsistent because it  
 424 defines a zero gradient in elevation head between the dual nodes. Since the vertical gradient in  
 425 elevation head between the dual nodes is zero the total flux rate after ponding now equals  
 426  $K_z (p_s - p_{ss})/l$ . Top-down saturation requires that this flux exceeds the vertical hydraulic  
 427 conductivity. Thus, reaching saturation at the topmost subsurface node ( $p_{ss} = 0$ ) requires  $p_s > l$ .  
 428 Therefore, top-down saturation will not occur if runoff occurs and if the surface water depths

429 remains smaller than the chosen coupling length. Indeed, it has been pointed out in other studies  
 430 that the coupling length should be smaller than the rill storage height [*Delfs et al.*, 2009; *Liggett et*  
 431 *al.*, 2012]. The zero vertical gradient in elevation head between the dual nodal also means that the  
 432 ~~required condition for ponding now becomes  $p_{ss} = -lq_R/K_z$ .~~ ponding occurs when  $p_{ss} > -lq_R/K_z$ .  
 433 This implies that ponding due to excess saturation occurs while the topmost subsurface node is not  
 434 yet saturated. This dual node approach has been compared to the common node approach in vertex-  
 435 centered schemes [*Liggett et al.*, 2012].

436 A second example is the dual node approach for cell-centered schemes as implemented in  
 437 MODHMS which uses an adapted pressure-saturation relationship for the topmost subsurface  
 438 nodes such that the topmost subsurface node only becomes fully saturated if hydraulic head at the  
 439 node rises above the land surface [*Liggett et al.*, 2013]. Since the topmost subsurface heads are  
 440 associated with the cell centroid, this dual node scheme defines a unit gradient in elevation head  
 441 at the land surface. However, the saturation value at the topmost node is associated with a location  
 442 at the land surface and not with the centroid of a discrete control volume. This has undesirable  
 443 consequences. Namely, saturating the topmost subsurface node ( $p_{ss} = l$ ) due to excess infiltration  
 444 requires that  $p_s > l$ . Indeed, when simulating excess infiltration with MODHMS, a very small  
 445 coupling length is needed to simulate top-down saturation due to excess infiltration. [*Gaukroger*  
 446 *and Werner*, 2011; *Liggett et al.*, 2013]. It can also be shown that ponding due to excess saturation  
 447 occurs while  ~~$0 < p_{ss} < l$ .~~  $p_{ss} > 0$ . But, because of the adapted pressure-saturation relationship this  
 448 means that ponding starts while the topmost subsurface node is not yet saturated. This dual node  
 449 approach has been compared to the common node approach in cell-centered schemes [*Liggett et*  
 450 *al.*, 2013].

451           The two comparison studies of Liggett et al. [Liggett et al., 2012; Liggett et al., 2013]  
452 indicate that the dual node approach is typically only competitive with the common node approach  
453 in terms of accuracy once the coupling length is very small. However, the requirement for a very  
454 small coupling length, is a logical consequence if the topmost subsurface nodal values are not  
455 taken as the mean values within discrete volumes. In essence, by choosing a very small coupling  
456 length this inconsistency is minimized. This contrasts with the consistent dual approach in which  
457 decreasing the coupling length for a given vertical discretization will result in more inaccurate  
458 simulation results as this would be numerically incorrect.

459           CATHY [Camporese et al., 2010] as well as the model of Morita and Yen [Morita and  
460 Yen, 2002] are examples of models which are neither based on the common node approach, nor a  
461 dual node approach. Both these models are conjunctive models in which the surface and subsurface  
462 flow are computed separately in a sequential fashion and in which coupling is established by  
463 matching the flow conditions along the surface-subsurface interface. A complete discussion is  
464 outside the scope of this paper, but it is worthwhile to mention that these models share some crucial  
465 characteristics with the consistent dual node approach. Although the two models are different, both  
466 models switch between appropriate boundary conditions along the surface-subsurface interface,  
467 such that infiltration fluxes are limited to the infiltrability. In both models the infiltration fluxes  
468 are computed while accounting for the unit vertical gradient in elevation head near the surface-  
469 subsurface interface. In addition, in both models ponding occurs when the infiltrability is  
470 exceeded.

## 471 5 Numerical experiments

### 472 5.1 Numerical model

473 To compare the consistent dual node approach with respect to the common node approach in terms  
474 of accuracy and computational efficiency numerical experiments are presented. These experiments  
475 are carried out with the model code DisCo. This model code can simulate coupled surface-  
476 subsurface flow with the dual node approach using a fully implicit or monolithic scheme [*de Rooij*  
477 *et al.*, 2013]. Subsurface flow is governed by the Richards' equation while surface flow is governed  
478 by the diffusive wave equation.

479 Starting from a dual node scheme, the implementation of a common node scheme is  
480 relatively straightforward. If the surface nodes are numbered last, a permutation vector can be  
481 constructed which gives the corresponding topmost subsurface node for each surface node. Then,  
482 the node numbering as used in the original dual node scheme can still be used to compute the  
483 surface and subsurface flow terms. Subsequently, using the permutation vector the surface and  
484 subsurface flow terms associated with a common node can be combined into the same row of the  
485 global matrix system. In addition, when using the common node approach, there is no need to  
486 evaluate exchange flow terms between the two flow domains. It is noted that the surface flow and  
487 subsurface flow computations are exactly the same irrespective of the coupling approach. As such  
488 the model permits to compare the two approaches in terms of accuracy as well as numerical  
489 efficiency.

490 An adaptive error-controlled predictor-corrector one-step Newton scheme [*Diersch and*  
491 *Perrochet*, 1999] is used in which a single user-specified parameter controls the convergence as  
492 well the time stepping regime. Although, this scheme may not be necessary the most efficient  
493 scheme, it ensures that time discretization error is the same irrespective of the applied coupling

494 approach. For brevity further details about the model are not discussed here and can be found  
495 elsewhere [de Rooij *et al.*, 2013].

## 496 **5.2 Hillslope scenarios**

497 The model code is applied to a set of three hillslope scenarios. Table 1 lists the abbreviations used  
498 in the figures to distinguish between the coupling approaches, and to distinguish between cell-  
499 centered and vertex-centered schemes. Each scenarios is solved using different but uniform  
500 vertical discretizations and  $\Delta z$  specifies the discretization of the primary grid. The first two  
501 simulation scenarios consider hillslope problems as designed by Sulis *et al.* [Sulis *et al.*, 2010].  
502 For the purpose of this study, a third scenario is considered in which the initial and boundary  
503 conditions are different to create a flooding wave across an unsaturated hillslope. The problems  
504 consist of a land surface with a slope of 0.05 which is underlain by a porous medium. The domain  
505 is 400 m long and 80 m wide. The subsurface is 5 m thick. In the direction of the length and in the  
506 direction of the width the discretization is 80 m. Different vertical discretizations are considered.  
507 The van Genuchten parameters are given by  $s_r = 0.2$ ,  $s_s = 1.0$ ,  $\alpha = 1 \text{ m}^{-1}$  and  $n = 2$ . The porosity is  
508 0.4 and the specific storage is  $10^{-4} \text{ m}^{-1}$ . The manning's roughness coefficients are given by  $3.3 \times$   
509  $10^{-4} \text{ m}^{-1/3} \text{ min}$ . The surface flow domain has a zero-gradient outflow condition. For the first two  
510 simulation scenarios the domain is recharged with an effective rainfall rate of  $3.3 \times 10^{-4} \text{ m/min}$  for  
511 a duration of 200 minutes and the initial water table depth is at a depth of 1.0 m below the land  
512 surface.

513 The first scenario considers excess saturation, the saturated conductivity equals  $6.94 \times 10^{-}$   
514  $4 \text{ m/min}$ . Figure 2 and 3 illustrates the simulated runoff and the number of Newton steps,  
515 respectively. Figure 4 and 5 illustrate the subsurface pressure heads at the topmost subsurface  
516 nodes and the water depths on the surface nodes. For the second scenario which considers excess

517 infiltration the saturated hydraulic conductivity equals  $6.94 \times 10^{-7}$  m/min. Figure 6 and 7 show the  
518 simulated runoff and the number of Newton steps, respectively. Figure 8 and 9 illustrate the  
519 subsurface pressure heads at the topmost subsurface nodes and the water depths on the surface  
520 nodes for the finest and the coarsest vertical discretization, respectively. In the third scenario a  
521 surface water flood wave crossing the hillslope in the downhill direction is simulated by applying  
522 a Neumann boundary condition of  $1.0 \text{ m}^3/\text{s}$  for a duration of 200 minutes to the surface nodes with  
523 the highest elevation. The initial water table is located at a depth of 1.5 m. The vertical saturated  
524 hydraulic conductivity equals  $6.94 \times 10^{-6}$  m/min. Figure 10 illustrates the differences in simulated  
525 runoff and Figure 11 illustrates the number of Newton steps of the model runs. Figure 12 and 13  
526 illustrate the subsurface pressure heads at the topmost subsurface nodes and the water depths on  
527 the surface nodes for the finest and the coarsest vertical discretization, respectively.

## 528 **6 Discussion**

### 529 **6.1 Accuracy**

530 As discussed by Ebel et al. [Ebel et al., 2009] and confirmed by others [Liggett et al., 2012] the  
531 dual node approach mimics the common node approach if the coupling length becomes sufficiently  
532 small. When comparing the consistent dual node approach and the common node approach a very  
533 similar observation applies. If the topmost subsurface cells are very thin, then the coupling length  
534 in the consistent dual node approach is very small. Also, if the topmost subsurface cells are  
535 sufficiently thin then the formulation of head continuity at the surface-subsurface interface in the  
536 common node approach is correct. Thus, the common node approach will mimic the consistent  
537 dual node approach. Indeed, the simulations results indicate that a relatively fine vertical

538 discretization yields similar results for the common node approach as well as for the consistent  
539 dual node approach (Figure 2a, 4a, 6a, 8a, 10a and 12a).

540 A relatively fine uniform vertical discretisation also enables to simulate sharp saturation  
541 fronts with the Richards' equation [*Pan and Wierenga, 1995; Ross, 1990*]. As such the simulation  
542 results based on the finest vertical discretization can be taken as reference solutions that enables  
543 comparisons of the coupling approaches when a coarser vertical discretization is used.

#### 544 **6.1.1 Excess saturation**

545 The simulation results of runoff due to excess saturation as obtained by the common node approach  
546 and the consistent dual node approach as depicted in Figure 2 illustrate that simulating excess  
547 saturation runoff is not significantly affected by the vertical discretization. This is because the time  
548 needed to reach fully saturated conditions in the subsurface is a simple function of the flow  
549 boundary conditions and the initial water content. It is thus expected that the vertical discretization  
550 does not significantly affect the simulation of excess saturation. Although the vertical  
551 discretization may affect the computed initial water content, this effect is usually negligible. ~~It has~~  
552 ~~been found in other studies that the vertical discretization has little effect on simulated runoff due~~  
553 ~~to excess saturation [*Sulis et al., 2010*]~~It has been found in other studies that the vertical  
554 discretization has little effect on simulated runoff due to excess saturation [*Kollet and Maxwell,*  
555 *2006; Sulis et al., 2010*].

#### 556 **6.1.2 Excess infiltration**

557 When simulating excess infiltration the common node approach requires fully saturated conditions  
558 at the topmost subsurface node for ponding to occur. However, top-down saturation associated  
559 with excess infiltration implies that reaching fully saturated conditions in the topmost subsurface  
560 discrete volumes should requires more time than reaching fully saturated conditions at the land



561 surface, especially if the vertical discretization is relatively coarse. It is thus expected that the  
562 common node approach delays runoff and that this delay increases for a coarser vertical  
563 discretization. In addition, if the saturation fronts are less sharp due to a relatively coarse vertical  
564 discretization, it takes more time to reach saturated conditions at the common node. This will  
565 further delay runoff. Indeed, the simulation results indicate clearly that runoff is delayed when  
566 using the common node approach, particularly if the vertical discretization is relatively coarse  
567 (Figure 6, 9a, 10 and 13a). It has also been found in other studies that the common node approach  
568 delays runoff due to excess infiltration if the vertical discretization is relatively coarse [*Sulis et al.*,  
569 2010].

570 As explained in Section 4.2, when using the consistent dual node approach, ponding due  
571 to excess infiltration occurs before reaching fully saturated conditions at the topmost subsurface  
572 node. More specifically, ponding occurs when the infiltrability is exceeded. Compared to the  
573 condition for ponding in the common node approach this is arguably more correct. Namely, if  
574 saturation occurs from the top-down then the saturation at a certain depth occurs later than  
575 saturation at the land surface. Indeed, simulation results indicate that when simulating excess  
576 infiltration the consistent dual node approach is less sensitive to the vertical discretization in  
577 comparison to the common node approach. This is clearly indicated in Figure 6b-d, 9a, 10b-d and  
578 13a. To further explain this difference in accuracy, it is emphasized that the spatial resolution only  
579 affects the accuracy of the flow computations when using the consistent dual node approach and  
580 that the formulation of head continuity at the interface remains correct. In contrast, when using the  
581 common node approach, if the spatial resolution is too coarse then this does not only affect the  
582 accuracy of the flow computations but in addition the formulation of head continuity becomes  
583 incorrect. It must be emphasized, however, that regardless of the applied coupling approach, the

584 vertical discretization must be relatively fine. As indicated by Figure 6b-d, 9a, 10b-d and 13a the  
585 difference between the simulated results and the reference solution increase for a coarser  
586 discretization. Eventually such differences will lead to unreasonable results regardless of the  
587 coupling approach.

588         It is interesting to note that An and Yu [*An and Yu, 2014*] also found that their model was  
589 less sensitive to the vertical discretization in comparison to ParFlow when simulating runoff due  
590 to excess infiltration. Whereas An and Yu [*An and Yu, 2014*] hypothesized that this difference in  
591 performance was related to using irregular grids instead of orthogonal grids as in ParFlow, it is  
592 argued here that this difference can be explained by the fact that both models use a different  
593 coupling approach.

594         Although the consistent dual node approach is less sensitive to the vertical discretization  
595 in comparison to the common node approach, it is useful to explain in detail how the vertical  
596 discretization affects the accuracy of the consistent dual node approach to the vertical  
597 discretization. A relatively coarse vertical discretization may result in an underestimation of the  
598 vertical pressure gradient at the land surface. This is because in a soil close to hydrostatic  
599 conditions the pressure heads increase with depth. Therefore, the infiltrability during the early  
600 stages of infiltration may be underestimated. If the applied flux rate is sufficiently large such that  
601 the underestimated infiltrability is exceeded, then runoff during the early stages will be  
602 overestimated. Figure 6d illustrates that the runoff as simulated with the cell-centered scheme, a  
603 relatively coarse vertical discretization and a consistent dual node approach is indeed  
604 overestimated at early times. During the later stages of infiltration the pressure head at the topmost  
605 subsurface node will be underestimated due to the combined effect of an underestimated  
606 infiltration rate and the overly diffused saturation fronts. This results in an overestimation of the

607 infiltration rate in the later stages. Thus at some time after ponding has started, it is expected that  
608 the amount of runoff is underestimated.

609         If the underestimated infiltrability is not exceeded, then the overly diffused saturation fronts  
610 resulting from a relatively coarse vertical discretization will eventually lead to an underestimation  
611 of pressure head at the topmost subsurface node and as such the infiltrability may be overestimated  
612 at later times. Consequently, when using the consistent dual node approach runoff due to excess  
613 infiltration may be delayed. However, the delay in runoff as simulated by the consistent dual node  
614 approach will only equal the delay in runoff as simulated by the common node approach in the  
615 limit when  $q_R/K_z$  goes to unity. Namely, as explained in Section 4.2 if  $q_R/K_z$  goes to unity, then the  
616 consistent dual node approach behaves similar as a common node approach. However, in general,  
617 if the consistent dual node approach delays runoff, this delay will be smaller than the delay in  
618 runoff as simulated by the common node approach.

619         Comparing Figure 12a and 13a it can be observed that if the vertical discretization is  
620 relatively coarse then a common node can act as an artificial barrier for a surface water wave  
621 advancing across an initially unsaturated subsurface domain. Namely, as the wave travels  
622 downstream the wave can only advance to the next common node once it is fully saturated. The  
623 effect of this artificial barrier is that the front of the surface water wave is steepened. In contrast,  
624 the consistent dual approach simulates a wave that becomes less steep as it advances downstream  
625 for relatively fine as well as relatively coarse vertical discretizations as depicted in Figure 13a.

626         As illustrated in Figure 6b-d, and 10b-d, if the coupling approach and the vertical  
627 discretization are identical, then the vertex-centered schemes are closer to the reference solution  
628 with respect to the cell-centered schemes. This difference results solely from the fact the primary  
629 mesh is the same for both schemes. As such the vertical extent of the topmost subsurface volumes

630 is twice as small when using the vertex-centered scheme. This difference in vertical grid resolution  
631 near the land surface explains the differences between the schemes.

## 632 **6.2 Computational efficiency**

633 The computational efficiency of the schemes is measured in terms of the number of Newton steps.  
634 The number of Newton steps equals the number of times that the linearized system of equations is  
635 solved and this number depends on the time step sizes as well as the number of failed Newton  
636 steps. It is emphasized that the measured efficiency depends crucially on the applied model code.  
637 Nonetheless, as shown in the following, the measured differences in efficiencies can be explained  
638 in terms of abrupt changes in how fast pressure heads near the surface-subsurface interface are  
639 evolving with time. Regardless of the type of scheme used to solve the non-linear flow equations,  
640 such abrupt changes are difficult to solve.

641         Once ponding occurs a surface-subsurface flow model will encounter significant numerical  
642 difficulties as surface flow terms are activated. In essence, the activation of these terms represents  
643 a discontinuity in flow behaviour which is challenging to resolve [*Osei-Kuffuor et al.*, 2014].  
644 Indeed, the Newton steps as depicted in Figure 3 and 7 indicate that simulations encounter  
645 difficulties at the moment of ponding. These figures also indicate that the consistent dual node  
646 approach can be more efficient in comparison to the common node approach.

### 647 **6.2.1 Excess saturation**

648 Just before the moment of ponding due to excess saturation, the rate of change in pressure heads  
649 at the topmost subsurface nodes is relatively high for both coupling approaches. This high rate is  
650 related to the shape of the water retention curve. Typically, the derivative of the saturation with  
651 respect to the pressure head goes to zero when approaching fully saturated conditions. Once  
652 ponding starts, the surface flow terms are activated and therefore the rate of changes in pressure

653 heads at the topmost subsurface nodes decreases drastically. Both approaches must handle this  
654 drastic change. However, from Figure 4b and 5b it can be observed that the rate of change  
655 decreases more abruptly when using the common node approach.

656         When using the common node approach the vertical hydraulic gradients in the subsurface  
657 are close to zero at the moment of ponding, since additional water volumes can only be  
658 accommodated by means of specific storage. This implies that the infiltration rate drops  
659 instantaneously at the moment of ponding. In contrast, in the dual node approach ponding starts  
660 when the infiltrability is exceeded. Thus at the moment of ponding, the infiltration rate is higher  
661 in comparison to the common node approach. After ponding this infiltration rate will decrease  
662 quickly as the hydraulic heads at the dual nodes equilibrate. This difference in the infiltration rate  
663 at the moment of ponding explains why the topmost subsurface hydraulic heads change more  
664 smoothly when using the dual node approach. If the vertical discretization is coarser, then the  
665 infiltration rate at the moment of ponding as computed with the consistent dual node approach is  
666 even higher and this results in a lower initial rate initial rate of change in water depth as depicted  
667 in Figure 5a.

668         The more abrupt changes in pressure heads at the common node in comparison to the  
669 changes in pressure heads at the dual nodes mean that solving the activation of ponding with the  
670 common node approach is more difficult. It is noted that the differences in the infiltration rates  
671 between the two coupling approaches only occur at the moment of ponding and directly thereafter  
672 when water depths are relatively small. Namely, quickly after ponding, the hydraulic heads at the  
673 dual nodes will equilibrate and after that the two coupling approaches will behave similar. This  
674 explains why these differences in infiltration rates do not significantly affect the accuracy of  
675 simulated runoff.

676     **6.2.2 Excess infiltration**

677     Figure 8, 9, 12 and 13 illustrate the evolution of pressure heads at dual nodes and common nodes  
678     when simulating excess infiltration. When applying the consistent dual approach, the net flux into  
679     a topmost subsurface cell will decrease once ponding occurs, because the applied flux rate will be  
680     partitioned between dual nodes (i.e. between the surface flow and subsurface flow domain). This  
681     occurs while the topmost subsurface node is not yet fully saturated. After ponding the infiltration  
682     rate decreases such that if the topmost subsurface node reaches fully saturated conditions the net  
683     flux into the topmost subsurface node is relatively small. In contrast, partitioning of the applied  
684     flux rate on a common node between the surface flow and subsurface domain starts when the  
685     common node reaches fully saturated conditions at this node. This means that just before ponding  
686     the rate of change in pressure head is relatively high as the common node is driven towards fully  
687     saturated conditions while the infiltration rate is relatively high. This means that similar to the  
688     excess saturation scenario the rate of change in pressure head at the common node is high just  
689     before ponding. At the moment of ponding, this rate must drop abruptly as surface flow terms are  
690     activated. This abrupt change explains why the common node approach is less efficient.

691             Figures 7 and 11 also indicate that a coarser vertical discretization only provides a  
692     significant gain in efficiency in terms of Newton steps when using the consistent dual node  
693     approach. When using the common node approach, a coarser discretization does not change the  
694     fact that the topmost subsurface node must reach fully saturated conditions for ponding to occur  
695     and that the infiltration rate is relatively high just before ponding. When using the consistent dual  
696     node approach, a coarser vertical discretization means that the saturation fronts are more diffused  
697     such that the flow problem becomes easier to solve.

698 Figure 8a and 9a illustrate that for the second simulation scenario, ponding occurs almost  
699 simultaneously at all the surface nodes. Figure 12a and 13a show that this is different for the third  
700 scenario where ponding occurs at different times as the flooding wave travels downstream. When  
701 Figure 11a is compared with Figure 12a and when Figure 11d is compared with Figure 13a, it is  
702 clear that the common node approach encounters difficulties around each time ponding starts at a  
703 surface node. Figure 11 shows that these difficulties are encountered for all discretizations. In  
704 contrast the consistent dual node approach has much less difficulties solving these difficulties. As  
705 discussed in Section 6.1.2. the common node approach may result in steepening the advancing  
706 wave. This implies that water depths will be changing more quickly. This presents an additional  
707 difficulty for solving this flow problem with the common node approach.

## 708 **7 Conclusions**

709 In this study it is shown that the dual node approach should be conceptualized and implemented  
710 as a one-sided finite differences approximation of the vertical hydraulic gradient at the land  
711 surface. This provides an important new insight into the coupling length. Namely, if the dual node  
712 approach is properly implemented then the coupling length is related to the vertical grid resolution.  
713 Thus, the coupling length does not represent an additional non-physical model parameter and  
714 therefore the dual node approach is not automatically a less physically based approach in  
715 comparison to the common node approach. Actually, this study shows if the vertical discretization  
716 is not sufficiently fine then the head continuity at the surface-subsurface interface is formulated  
717 more correctly in the consistent dual node scheme. This difference in formulation has  
718 consequences for how both approaches compare in terms of accuracy and efficiency.

719 Numerical experiment indicate that the consistent dual node approach is equally accurate  
720 or more accurate than the common node approach. It has been shown that in comparison to the  
721 common node approach the consistent dual node approach is less sensitive to the vertical  
722 discretization when simulating excess infiltration. However, the practical advantage of the  
723 consistent dual node approach in terms of accuracy is limited. Namely, if the vertical discretization  
724 is refined, both approaches will converge to more accurate and eventually similar results when  
725 simulating excess infiltration. When simulating excess saturation both approaches yield similar  
726 results even if the vertical discretization is relatively coarse.

727 Nonetheless, even though the advantage of the consistent dual node approach in terms of  
728 accuracy is limited, the fact that the consistent dual node approach is equally or more accurate than  
729 the common node approach is a significant finding. Namely, this finding is different from the  
730 commonly held view that a dual node approach is most accurate if it mimics the common node  
731 approach. Moreover, it also illustrates clearly that the consistent dual node approach is not similar  
732 to a common node approach.

733 Numerical experiment indicate that the consistent dual node approach can be more efficient  
734 than the common node approach while being equally or more accurate than the common node  
735 approach. It has been shown that this difference in efficiency is related to abrupt changes in the  
736 evolution of pressure heads around the moment that ponding is initiated.

737 Based on the findings in this study the models of An and Yu [*An and Yu*, 2014] and Kumar  
738 et al. [*Kumar et al.*, 2009] are expected to have some advantages with respect to models that are  
739 based on the common node approach. This is because these models are based on a consistent dual  
740 node approach. Moreover, given a model that uses an alternative dual node approach, it is relatively  
741 straightforward to implement the numerically more correct consistent dual node approach.



742

743       **Acknowledgements**

744       This research was funded by the Carl. S. Swisher Foundation.

745

746       **References**

- 747       An, H., and S. Yu (2014), Finite volume integrated surface- subsurface flow modeling on  
748       nonorthogonal grids, *Water Resources Research*, 50(3), 2312-2328.
- 749       Blazek, J. (2005), *Computational fluid dynamics: Principles and applications* *Computational fluid*  
750       *dynamics: Principles and applications*, Elsevier.
- 751       Camporese, M., C. Paniconi, M. Putti, and S. Orlandini (2010), Surface-subsurface flow modeling  
752       with path-based runoff routing, boundary condition-based coupling, and assimilation of  
753       multisource observation data, *Water Resources Research*, 46.
- 754       De Rooij, R., W. Graham, and R. Maxwell (2012), A particle-tracking scheme for simulating  
755       pathlines in coupled surface-subsurface flows, *Advances in Water Resources*.
- 756       de Rooij, R., P. Perrochet, and W. Graham (2013), From rainfall to spring discharge: Coupling  
757       conduit flow, subsurface matrix flow and surface flow in karst systems using a discrete-continuum  
758       model, *Advances in Water Resources*, 61, 29-41.
- 759       Delfs, J. O., C. H. Park, and O. Kolditz (2009), A sensitivity analysis of Hortonian flow, *Advances*  
760       *in Water Resources*, 32(9), 1386-1395.
- 761       Diersch, H. J. G., and P. Perrochet (1999), On the primary variable switching technique for  
762       simulating unsaturated-saturated flows, *Advances in Water Resources*, 23(3), 271-301.
- 763       Ebel, B. A., B. B. Mirus, C. S. Heppner, J. E. VanderKwaak, and K. Loague (2009), First-order  
764       exchange coefficient coupling for simulating surface water-groundwater interactions: parameter  
765       sensitivity and consistency with a physics-based approach, *Hydrological Processes*, 23(13), 1949-  
766       1959.
- 767       Gaukroger, A. M., and A. D. Werner (2011), On the Panday and Huyakorn surface-subsurface  
768       hydrology test case: analysis of internal flow dynamics, *Hydrological Processes*, 25(13), 2085-  
769       2093.
- 770       Hillel, D. (1982), *Introduction to soil physics*, Academic press New York.
- 771       Kolditz, O., and H. Shao (2010), OpenGeoSys, Developer-Benchmark-Book, OGS-DBB 5.04,  
772       Helmholtz Centre for Environmental Research (UFZ).
- 773       Kollet, S. J., and R. M. Maxwell (2006), Integrated surface-groundwater flow modeling: A free-  
774       surface overland flow boundary condition in a parallel groundwater flow model, *Advances in*  
775       *Water Resources*, 29(7), 945-958.
- 776       Kumar, M., C. J. Duffy, and K. M. Salvage (2009), A Second-Order Accurate, Finite Volume-  
777       Based, Integrated Hydrologic Modeling (FIHM) Framework for Simulation of Surface and  
778       Subsurface Flow, *Vadose Zone Journal*, 8(4), 873-890.
- 779       Liggett, J. E., A. D. Werner, and C. T. Simmons (2012), Influence of the first-order exchange  
780       coefficient on simulation of coupled surface-subsurface flow, *Journal of Hydrology*, 414, 503-515.

781 Liggett, J. E., M. J. Knowling, A. D. Werner, and C. T. Simmons (2013), On the implementation  
782 of the surface conductance approach using a block-centred surface-subsurface hydrology model,  
783 *Journal of Hydrology*, 496, 1-8.

784 Morita, M., and B. C. Yen (2002), Modeling of conjunctive two-dimensional surface-three-  
785 dimensional subsurface flows, *Journal of Hydraulic Engineering-Asce*, 128(2), 184-200.

786 Moukalled, F., L. Mangani, and M. Darwish (2016), *The Finite Volume Method in Computational*  
787 *Fluid Dynamics*, Springer.

788 Osei-Kuffuor, D., R. M. Maxwell, and C. S. Woodward (2014), Improved numerical solvers for  
789 implicit coupling of subsurface and overland flow, *Advances in Water Resources*, 74, 185-195.

790 Pan, L., and P. J. Wierenga (1995), A transferred pressure head based approach to solve Richards  
791 equation for variably saturated soils, *Water Resources Research*, 31(4), 925-931.

792 Panday, S., and P. S. Huyakorn (2004), A fully coupled physically-based spatially-distributed  
793 model for evaluating surface/subsurface flow, *Advances in Water Resources*, 27(4), 361-382.

794 Ross, P. J. (1990), Efficient numerical methods for infiltration using Richards equation, *Water*  
795 *Resources Research*, 26(2), 279-290.

796 Sulis, M., S. B. Meyerhoff, C. Paniconi, R. M. Maxwell, M. Putti, and S. J. Kollet (2010), A  
797 comparison of two physics-based numerical models for simulating surface water-groundwater  
798 interactions, *Advances in Water Resources*, 33(4), 456-467.

799 Therrien, R., R. G. McLaren, E. A. Sudicky, and S. M. Panday (2010), HydroGeoSphere-a three-  
800 dimensional numerical model describing fully-integrated subsurface and surface flow and solute  
801 transport (draft), Groundwater Simulations Group, University of Waterloo.

802 VanderKwaak, J. E. (1999), Numerical simulation of flow and chemical transport in integrated  
803 surface-subsurface hydrologic systems, University of Waterloo.

804 Yeh, G.-T., D.-S. Shih, and J.-R. C. Cheng (2011), An integrated media, integrated processes  
805 watershed model, *Computers & Fluids*, 45(1), 2-13.

806 Zienkiewicz, O., R. Taylor, and J. Zhu (2005), *The finite element method: its basis and*  
807 *fundamentals*. 2005, edited, Butterworth-Heinemann.

808  
809  
810  
811  
812  
813

abbreviation	meaning
cc	cell-centered
vc	vertex-centered
dn	dual node

814

815 Table 1: Abbreviations as used in the figures.

816

817

818

819

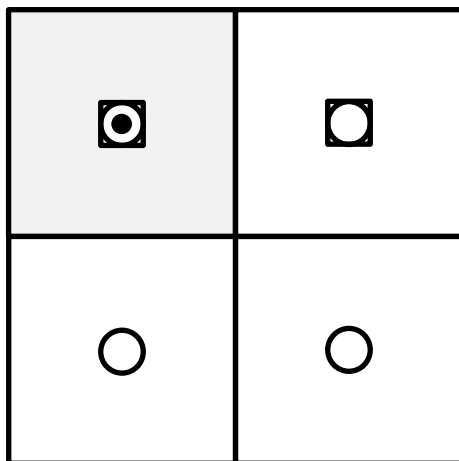
820

821

822

823

a)



824

825

826

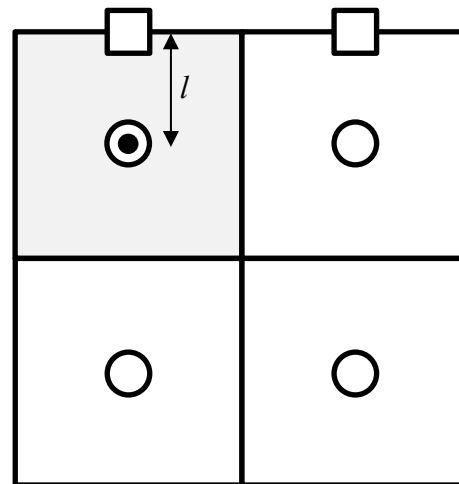
827

828

829

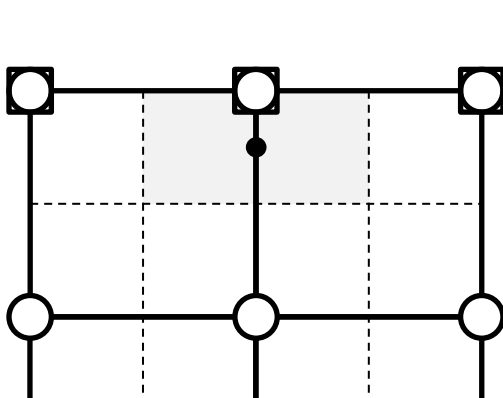
830

b)



831

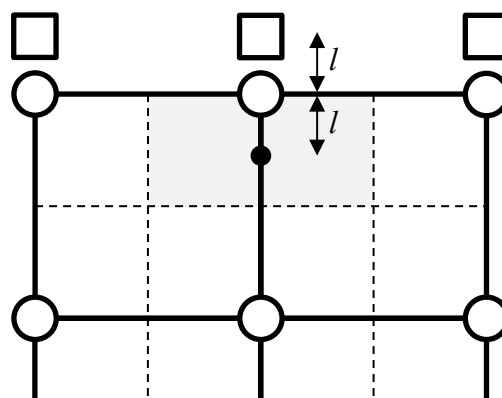
c)



832

833

d)



834

835

836

837

838

839

840

841

842

843 Figure 1: a) Common nodes in cell-centered schemes. b) Dual nodes in cell-centered-centered  
844 schemes. c) Common nodes and co-located dual nodes in vertex-centered schemes. d) Dual nodes  
845 in vertex-centered schemes (not co-located). The white squares and white circles represent surface  
846 and subsurface nodes, respectively. The solid and dashed lines represent the primary mesh and the  
847 dual mesh, respectively. The grey-shaded area is a topmost discrete volume as associated with a  
848 topmost subsurface node. The black dot represents the centroid of this volume. The coupling length  
849  $l$  as depicted in this figure applies to the consistent dual node approach.

850

851

852

853

854

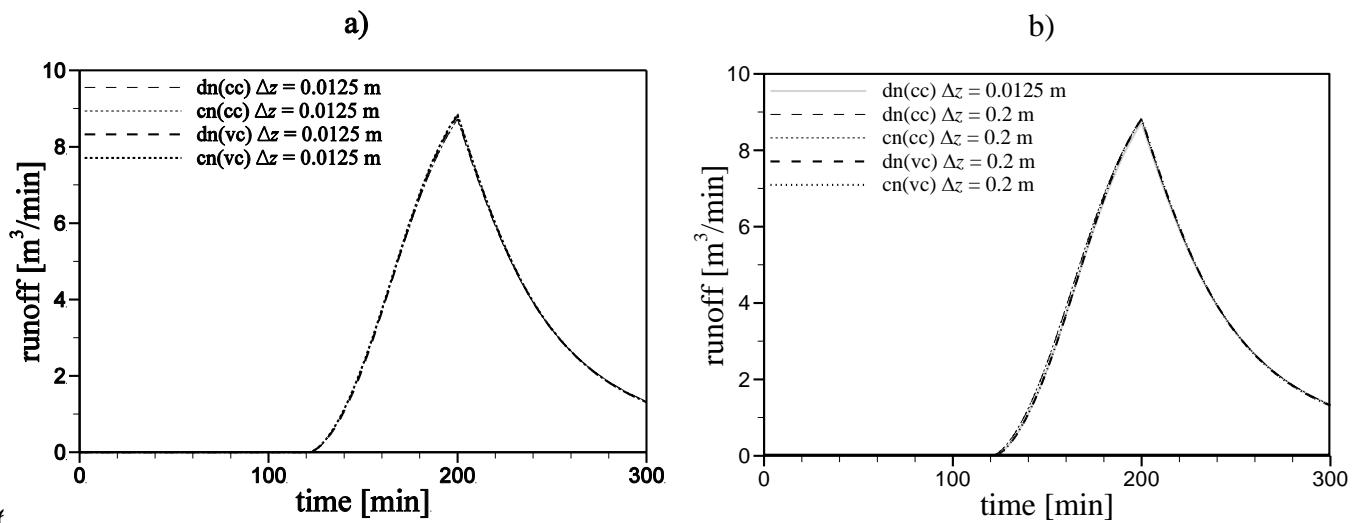
855

856

857

858

859

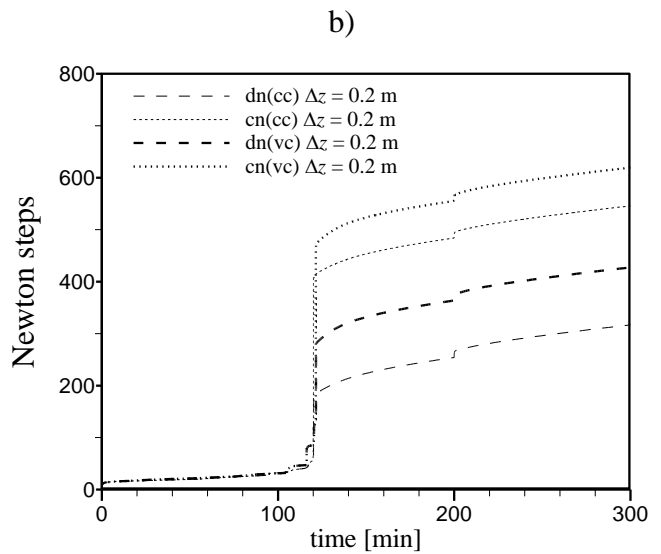
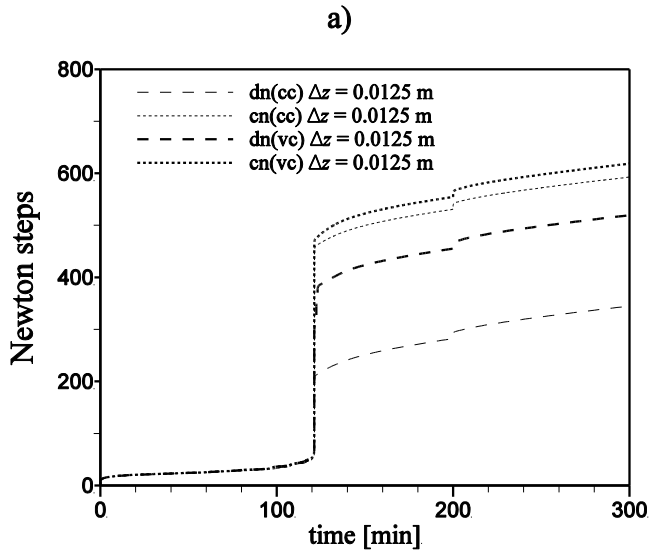


860

861 Figure 2: Outflow response for excess saturation on a hillslope (first scenario) using different

862 vertical discretizations.

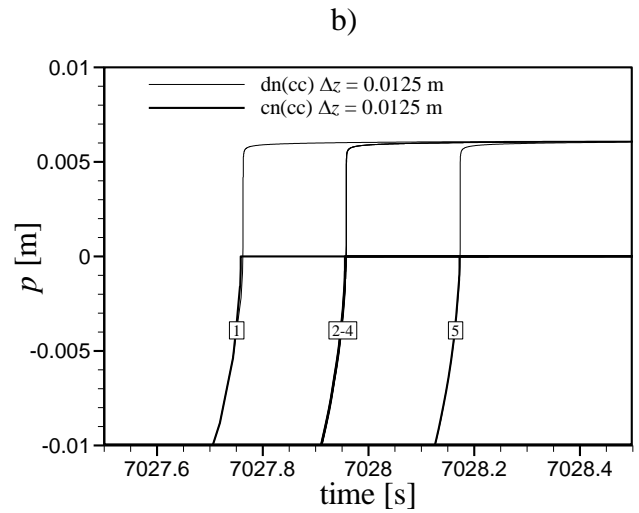
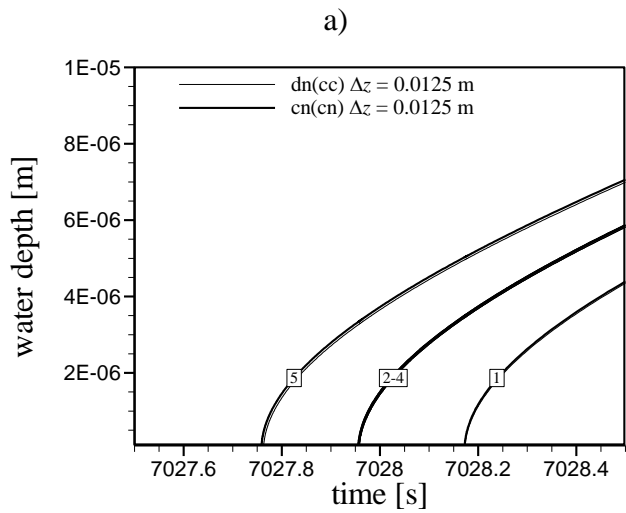
863



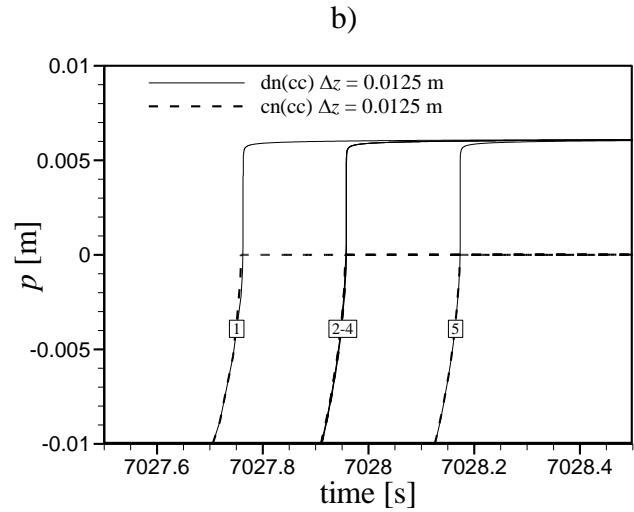
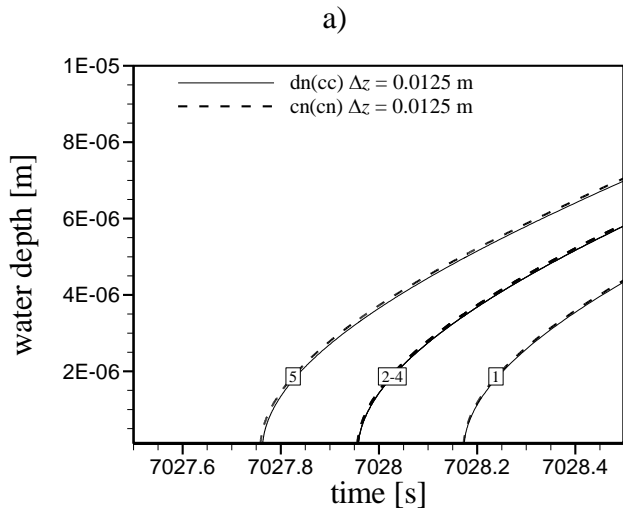
864 .

865 Figure 3: Number of Newton steps for excess saturation on a hillslope (first scenario) using  
 866 different vertical discretizations.

867

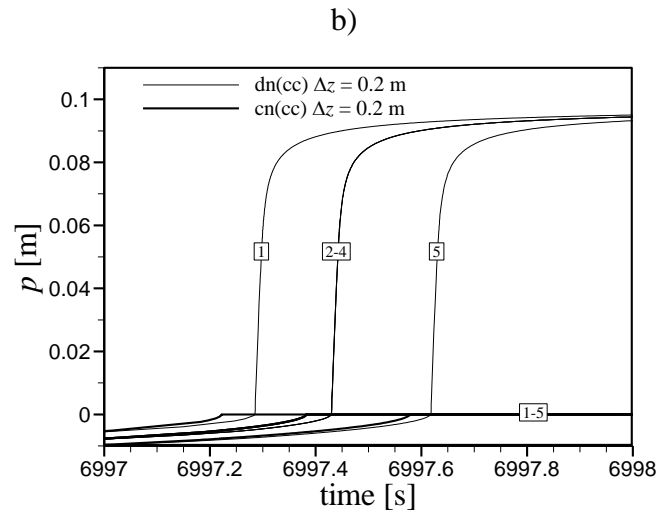
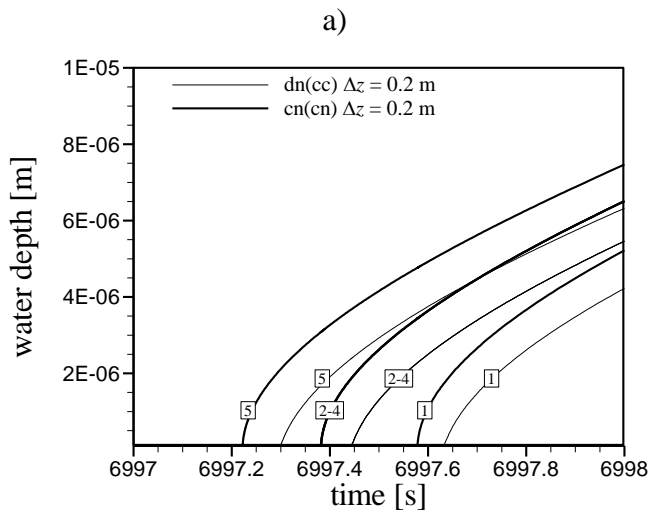


868 .

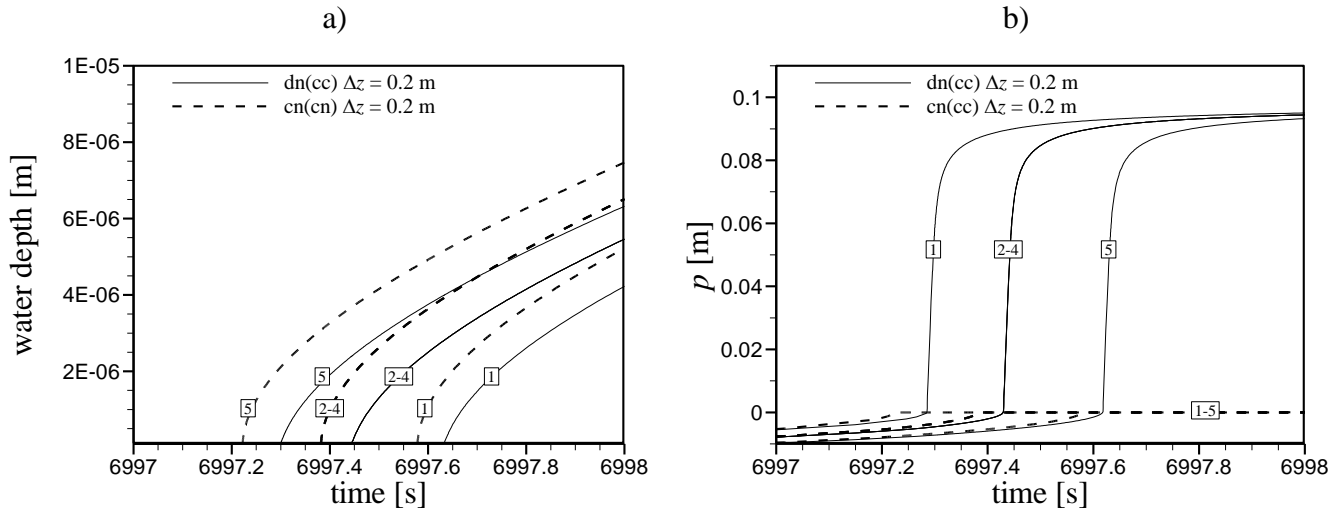


80

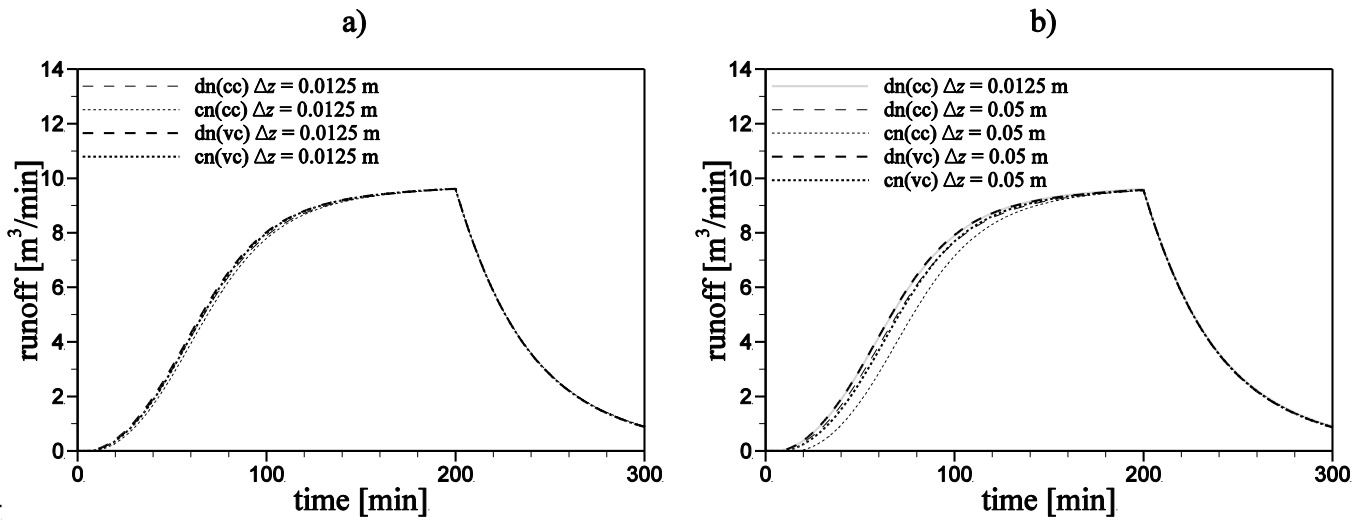
870 Figure 4: Simulated values at the common nodes for excess saturation on a hillslope (first scenario)  
 871 with a cell-centered scheme and  $\Delta z = 0.0125$  m. a) Water depths. b) Pressure heads. Nodes are  
 872 numbered 1-5 in the down-slope direction.



81

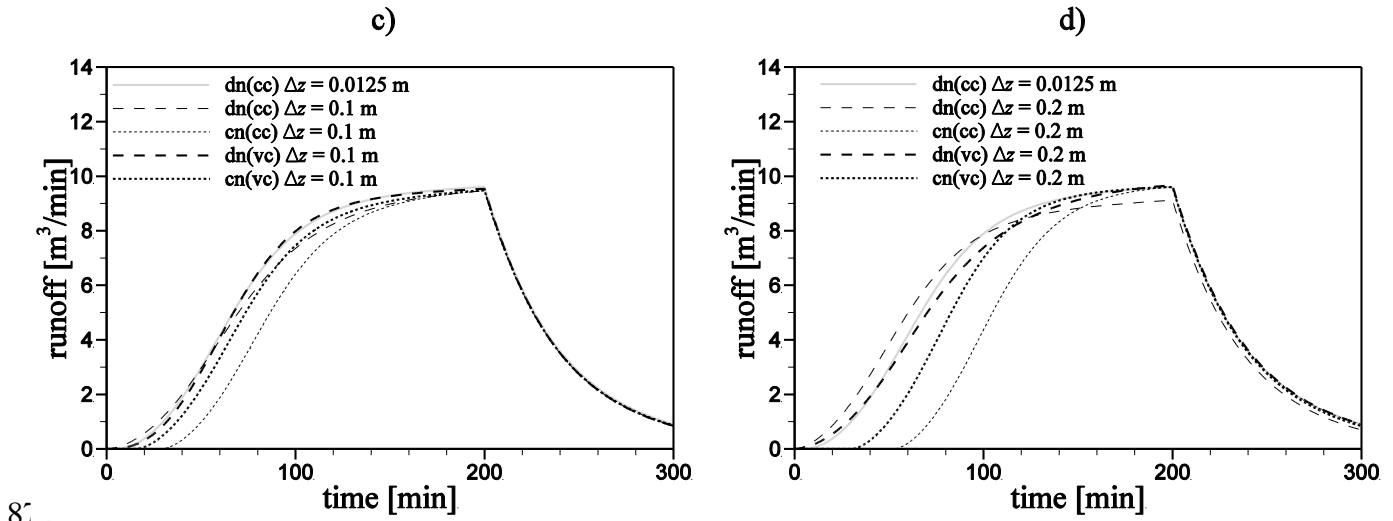


875 Figure 5: Simulated values for excess saturation on a hillslope (first scenario) with a cell-centered  
 876 scheme and  $\Delta z = 0.2$  m. a) Water depths at the surface nodes. b) Pressure heads at the topmost  
 877 subsurface nodes. Nodes are numbered 1-5 in the down-slope direction.



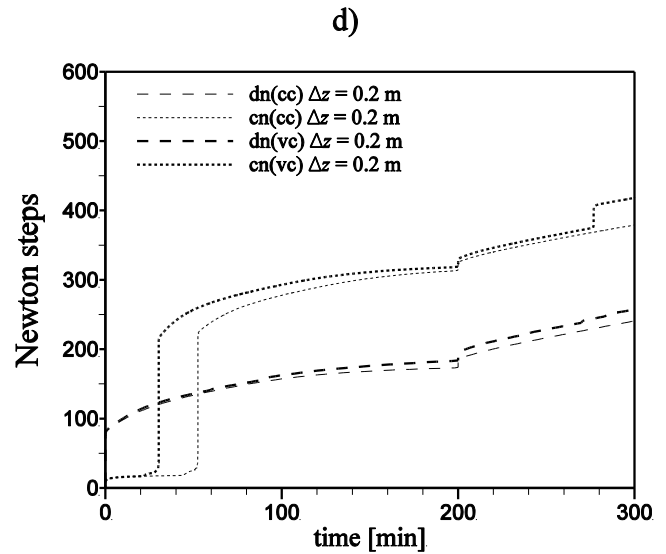
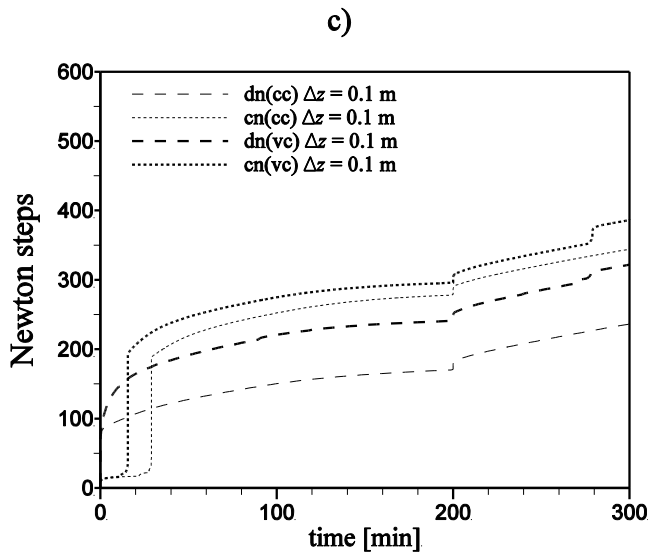
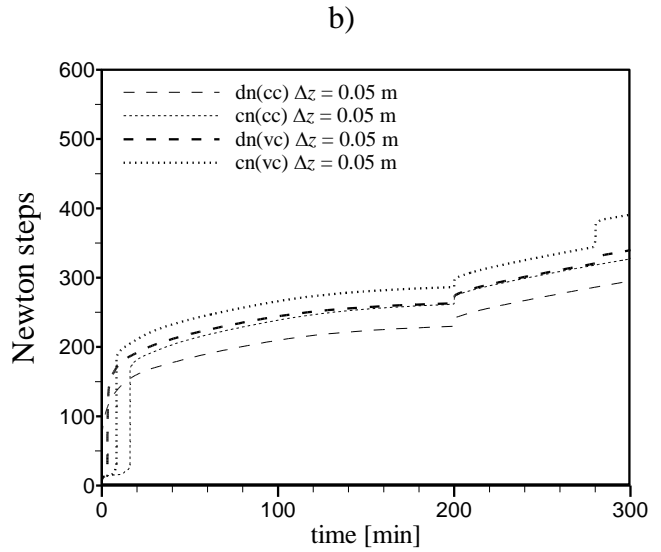
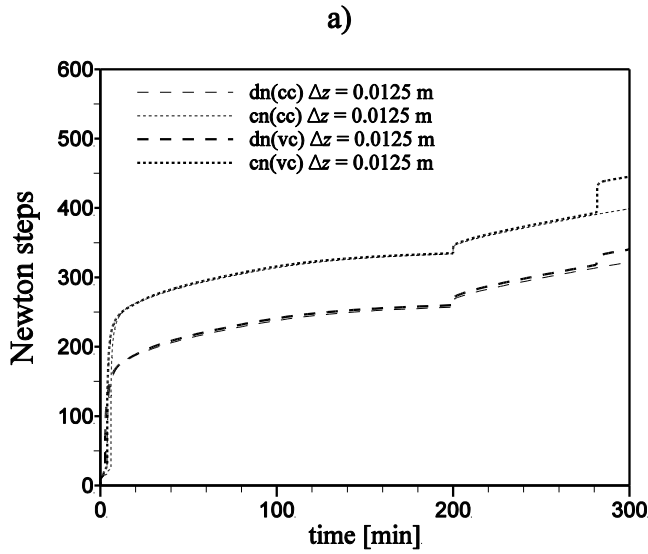
878





87. .  
 880 Figure 6: Outflow response for excess infiltration on a hillslope (second scenario) using different  
 881 vertical discretizations.

882  
 883  
 884  
 885  
 886



888

889

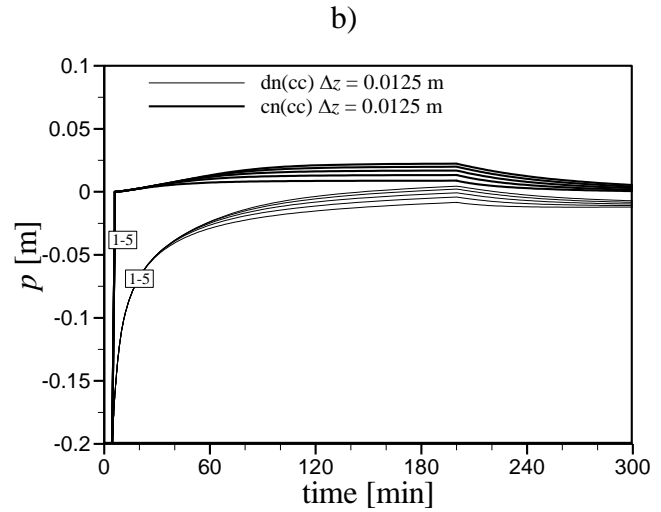
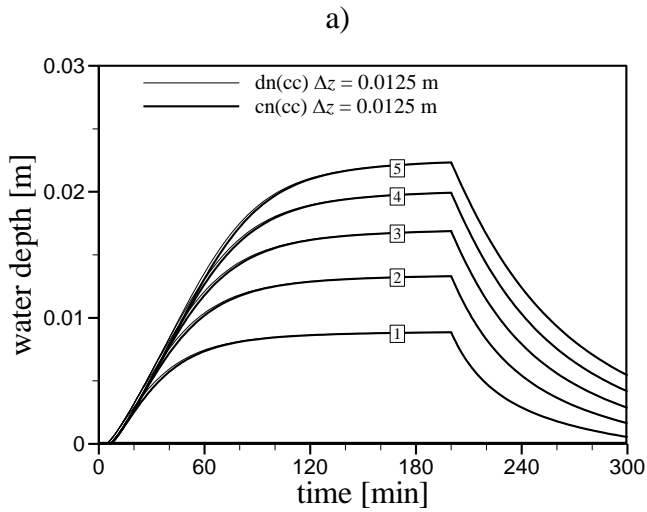
889 Figure 7: The total number of Newton steps for excess infiltration (second scenario) on a hillslope  
 890 using different vertical discretizations.

891

892

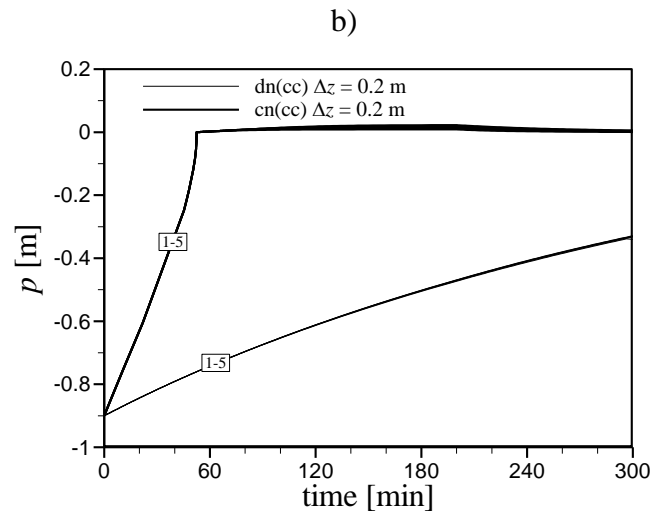
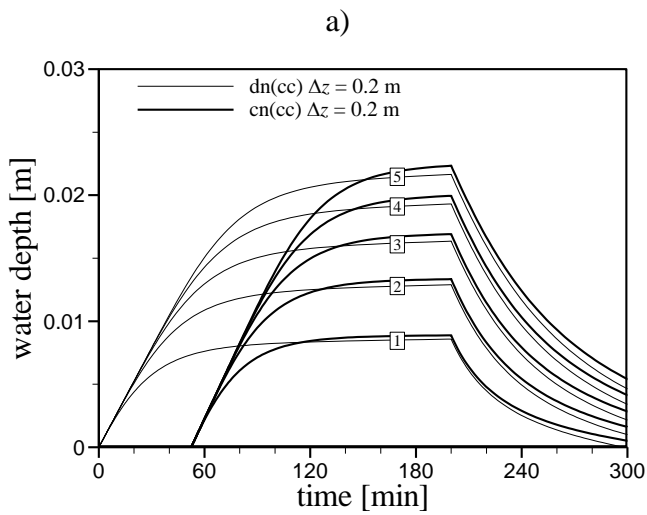
893

894

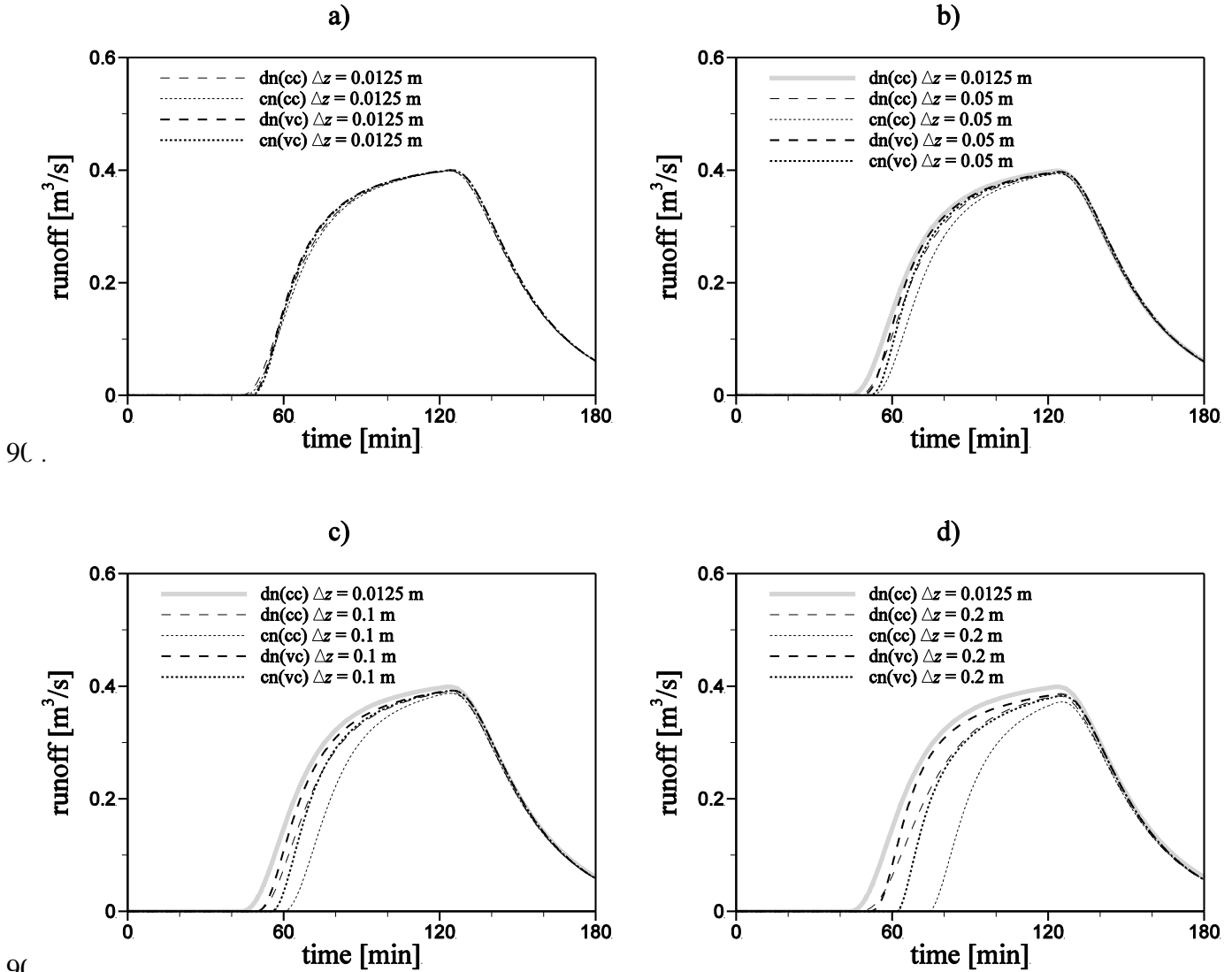


896 Figure 8: Simulated values at the common nodes for excess infiltration on a hillslope (second  
 897 scenario) with a cell-centered scheme and  $\Delta z = 0.0125$  m. a) Water depths. b) Pressure heads.  
 898 Nodes are numbered 1-5 in the down-slope direction.

899



901 Figure 9: Simulated values for excess infiltration on a hillslope with a cell-centered scheme  
 902 (second scenario) and  $\Delta z = 0.2$  m. a) Water depths at the surface nodes. b) Pressure heads at the  
 903 topmost subsurface nodes. Nodes are numbered 1-5 in the down-slope direction.



906 Figure 10: Outflow response for flooding an unsaturated hillslope using different vertical  
 907 discretizations.

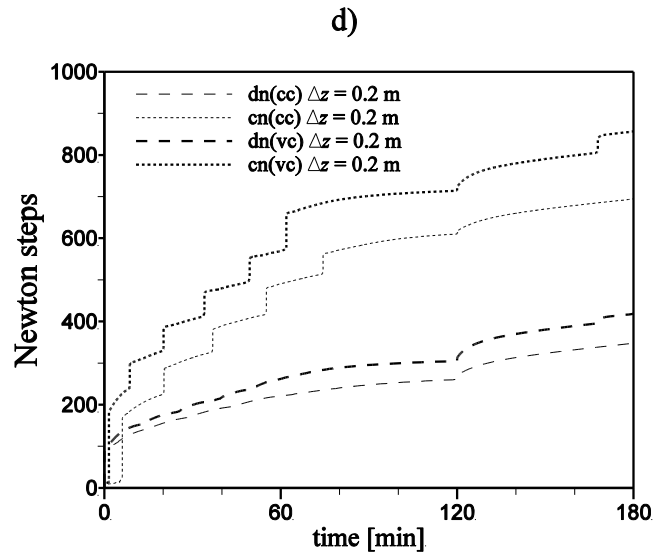
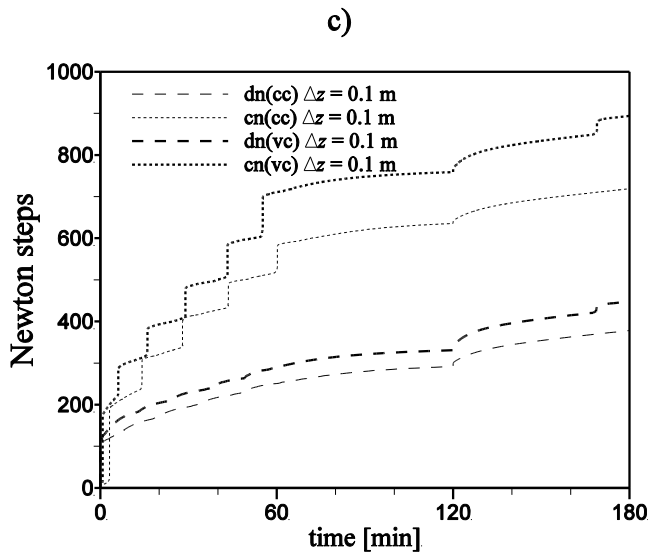
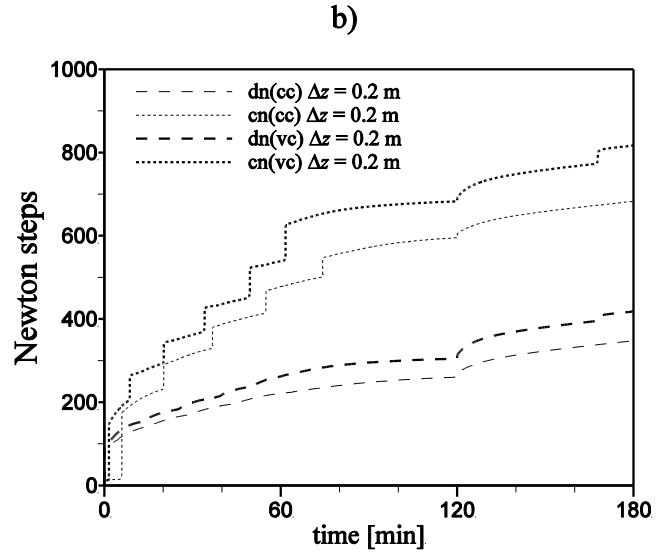
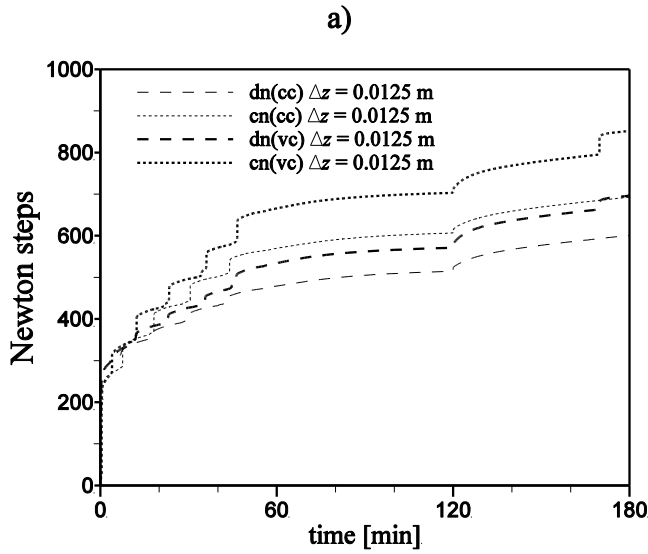
908

909

910

911

912



91

91

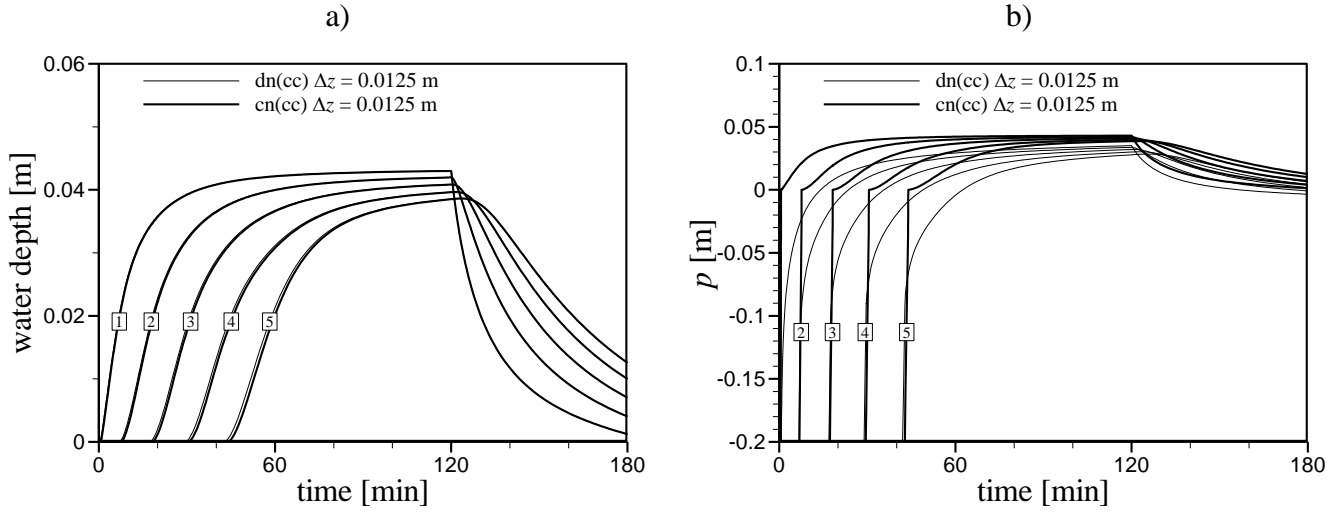
915 Figure 11: Number of Newton steps for flooding an unsaturated hillslope using different vertical  
 916 discretizations.

917

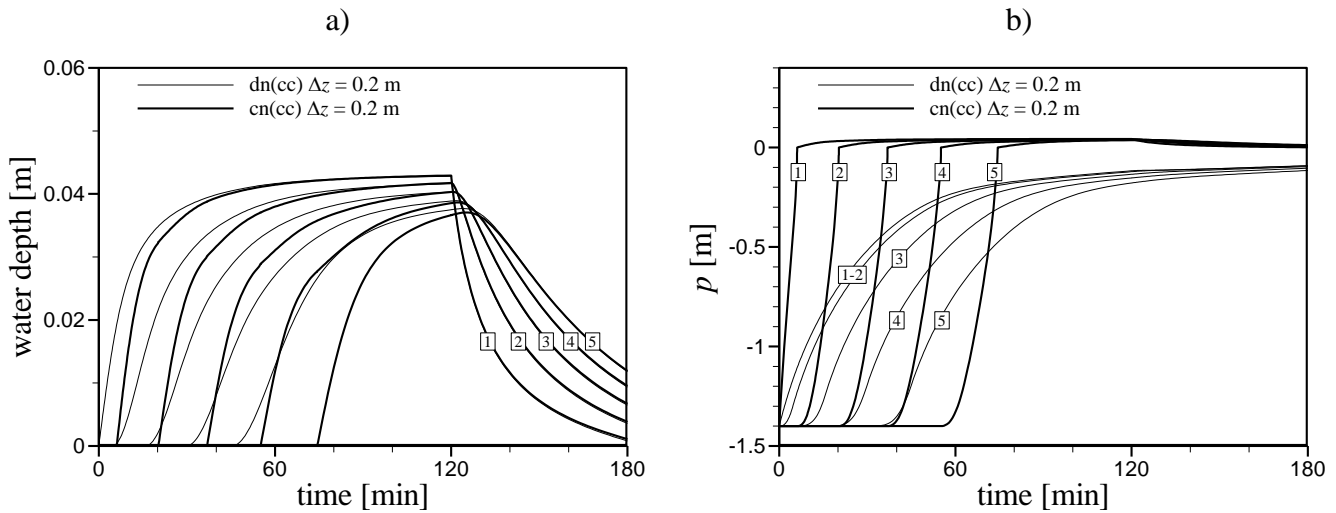
918

919

920



922 Figure 12: Simulated values for excess infiltration (third scenario) on a hillslope with a cell-  
 923 centered scheme and  $\Delta z = 0.0125$  m. a) Water depths at the surface nodes. b) Pressure heads at the  
 924 topmost subsurface nodes. Nodes are numbered 1-5 in the down-slope direction).



926 Figure 13: Simulated values for excess infiltration (third scenario) on a hillslope with a cell-  
 927 centered scheme and  $\Delta z = 0.2$  m. a) Water depths at the surface nodes. b) Pressure heads at the  
 928 topmost subsurface nodes. Nodes are numbered 1-5 in the down-slope direction).